

Sub-cellular level resolution of common genetic variation in the photoreceptor layer identifies continuum between rare disease and common variation

Hannah Currant^{1,2}, Tomas W Fitzgerald¹, Praveen J Patel³, Anthony P Khawaja³, UK Biobank Eye and Vision Consortium, Andrew R Webster³, Omar A Mahroo^{3,4,5*}, Ewan Birney^{1*}

1 European Molecular Biology Laboratory, European Bioinformatics Institute, Cambridge, UK

2 Novo Nordisk Foundation Center for Protein Research, Faculty of Health and Medical Sciences, University of Copenhagen, Copenhagen, Denmark

3 NIHR Biomedical Research Centre, Moorfields Eye Hospital NHS Foundation Trust UCL Institute of Ophthalmology, London, UK

4 Section of Ophthalmology, King's College London, St Thomas' Hospital Campus, London, UK

5 Physiology, Development and Neuroscience, University of Cambridge, Cambridge, UK

* Corresponding authors, o.mahroo@ucl.ac.uk and birney@ebi.ac.uk

Abstract

Photoreceptor cells (PRCs) are the light-detecting cells of the retina. Such cells can be non-invasively imaged using optical coherence tomography (OCT) which is used in clinical settings to diagnose and monitor ocular diseases. Here we present the largest genome-wide association study of PRC morphology to date utilising quantitative phenotypes extracted from OCT images within the UK Biobank. We discovered 111 loci associated with the thickness of one or more of the PRC layers, many of which had prior associations to ocular phenotypes and pathologies. We further identified 10 genes associated with PRC thickness through gene burden testing using exome data. In both cases there was a significant enrichment for genes involved in rare eye pathologies, in particular retinitis pigmentosa. There was evidence for an interaction effect between common genetic variants, *VSX2* involved in eye development and *PRPH2* known to be involved in retinal dystrophies. We further identified a number of genetic variants with a differential effect across the macular spatial field. Our results suggest a continuum between normal and rare variation which impacts retinal structure, sometimes leading to disease.

Introduction

The retina is a layered structure at the back of the eye, responsible for receiving light stimulus and converting it to neurological signal which is interpreted by the visual system of the brain. Each retinal layer comprises different cells that are responsible for particular stages of the signal conversion process. The central area of the retina is termed the macula, and has a valley like structure. At the centre of the macula, the bottom of the valley structure, is the fovea which is the area of the retina responsible for highest acuity vision [1]. The retina can be imaged using optical coherence tomography

(OCT). OCT produces high resolution, three-dimensional representations of the retina in which the different retinal layers and macular structure can be identified (fig. 1A). OCT is a non-invasive imaging method commonly used in the clinic to diagnose and monitor a number of ophthalmic conditions [2].

The photoreceptor cells (PRCs) are found towards the back of the eye within the retina, backed by the retinal pigment epithelium layer (RPE) (fig. 1A), and are responsible for detecting light photons and generating electrical response through the process of phototransduction. They consist of two main types, the rods and cones. Rods are responsible for vision in low light but offer lower visual acuity and lack colour definition. Cones are active in higher light levels, and confer colour and high acuity vision. The cones are densely populated at the centre of the retina, the fovea, where there are no rods. Conversely, rods are most densely populated more peripherally, where cone density is low. The PRC layer can be further divided into three component intracellular layers; the outer nuclear layer (ONL), which comprises the cell body of the PRC, including the cell nucleus; the inner segment (IS), which contains both the PRC's mitochondria and ribosomes required for photopigment assembly; and the outer segment (OS), which interfaces with the RPE and contains the stacked membranes in which photopigments are stored.

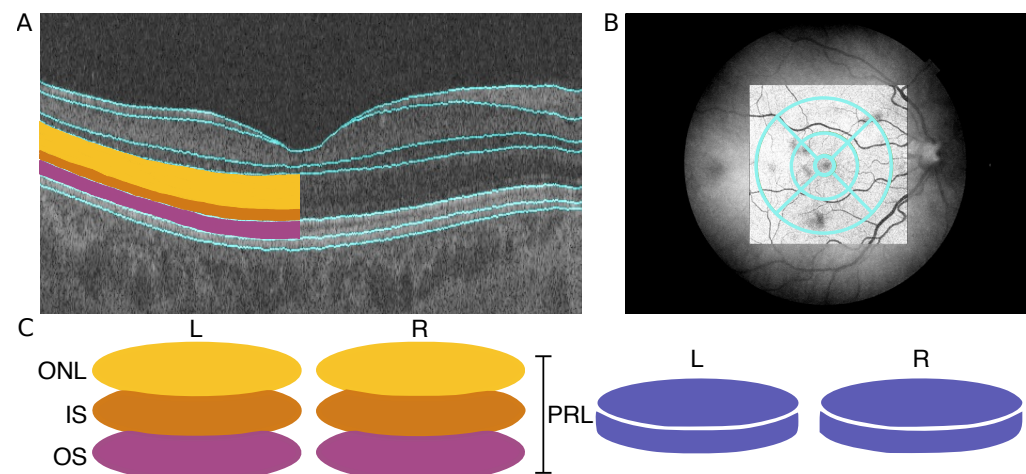


Fig 1. Data available from OCT images to describe morphology of the photoreceptor cell layer. (A) An optical coherence tomography (OCT) image of the cross-section of the retina. The layers are segmented, outlined in blue, by the Topcon advanced boundary software (TABS). On the left-hand side of the image, the PRC layers have been shaded: The outer nuclear layer (ONL) in yellow, the inner segment (IS) in orange and the outer segment (OS). (B) The early treatment of diabetic retinopathy study (ETDRS) segmentation grid super imposed on a fundus image of the retina. The ETDRS grid is composed of nine segments arranged in a bulls-eye. (C) A schematic of the data utilised to describe PRC morphology as an input phenotype in genome-wide association studies (GWAS). The ONL, IS and OS, combined, comprise the photoreceptor layer (PRL).

There are numerous pathologies, both rare and common, that affect the morphology of the PRCs. Notably, age-related macular degeneration (AMD) is defined by the accumulation of lipid deposits, known as drusen, under the RPE. This causes damage to the RPE and subsequently degradation of the PRCs [3]. AMD causes progressive and irreversible loss of visual function, and is a major cause of blindness in older people. [4].

Many retinal dystrophies affect the photoreceptors [5]. These rare inherited disorders are due to highly penetrant mutations in genes expressed in PRCs or less commonly the

RPE, resulting in retinal dysfunction with or without degeneration of the outer retinal layers. These can affect predominantly the central retina (macular dystrophies), the rod photoreceptors (rod-cone dystrophy or retinitis pigmentosa), or the cone photoreceptors (cone and cone-rod dystrophies). Though individually rare, taken together these diseases are a major cause of blindness in children and working age adults.

There have been previous studies on retinal morphology with known associations to age, sex, and ethnicity [6, 7]. Previous studies have further looked at the genetic variation underlying the overall retinal thickness [8] and the thickness of the inner retinal layers [9]. These studies identified loci with prior associations to general retinal development and ophthalmic disease.

In this paper, we utilise data within the UK Biobank to interrogate how genetic variation affects PRC morphology using quantitative phenotypes extracted from OCT images. The UK Biobank provides a large-scale rich resource of both genotypic and phenotypic data. Here we conduct genome-wide association studies (GWAS) of the thickness of the component PRC layers, the ONL, IS and OS. Following meta analysis of the three PRC layers, 111 loci are significantly associated with the thickness of one or more PRC layers. These loci include variants with prior associations to ophthalmic phenotypes, including ophthalmic diseases. We further explored the genetic variation of the morphology of the retina at a higher resolution by considering the retinal layer thickness in different concentric areas of the macula. This identified a number of loci that appear to differentially affect PRC morphology across the retinal field. Interestingly, several of these loci have prior associations to retinal diseases whose pathological action bears similarity with the spatial variation in genetic effect on morphology. Further analysis utilising the exome sequence data identified 10 genes associated with the thickness of one or more of the PRC layers. Several of these genes also had prior associations to ocular phenotypes. Additional analysis identified interaction between two of the common genetic variants, *VSX2* and *PRPH2*, affecting outer retinal thickness. We further explored the spatial genetic effect of our discovered genetic variants to capitalise on more of the available dimensionality of the phenotype data.

Methods

Ethics Statement

The UK Biobank study was conducted with the approval of the North-West Research Ethics Committee (ref 06/MRE08/65), in accordance with the principles of the Declaration of Helsinki, and all participants gave written informed consent. The research presented here has been conducted using the UK Biobank Resource under Application Number 2112.

UK Biobank Data

The UK Biobank is a cohort comprising ~500,000 individuals recruited through the NHS registry at age 40-69 from across the UK. Individuals were not selected on the basis of having disease, resulting in a broad cross-section of the UK population. For all participants, a number of baseline physical measurements were taken and an extensive questionnaire completed comprising information on lifestyle, demographic and socioeconomic factors. Additionally, blood and urine samples were collected and further tests including a heel-bone ultrasound, bio-impedance, hand-grip strength, spirometry, blood pressure and several cognitive tests were performed. Each individual was further

genotyped and exome sequenced. The participants also agreed to ongoing linkage of their medical records [10].

Ophthalmic Measurements and Optical Coherence Tomography

A subset of 132,041 participants completed an eye examination. The measures collected included best corrected visual acuity using a logarithm of the minimum angle of resolution (logMAR) chart (Precision Vision, LaSalle, Illinois, USA). Visual acuity was measured with participants wearing their distance glasses at 4m, or at 1m if a participant was unable to read letters at 4m. Participants were asked to read from the top of the chart downwards, with the test terminated when two or more letters were read incorrectly. Further, refractive error was measured using a Tomey RC-5000 auto refraktometer (Tomey Corp., Nagoya, Japan) [11]. For each eye, up to 10 measurements were taken and the most reliable measure was automatically recorded. Intraocular pressure (IOP) was measured using an Reichert Ocular response Analyzer [12] from which corneal compensated IOP was calculated that accounts for rigidity of the cornea [13].

Optical Coherence Tomography Imaging Data

A further subset of 67,321 individuals underwent Spectral Domain Optical Coherence Tomography (SD-OCT) imaging. OCT imaging was conducted using the the Topcon 3D OCT1000 Mark II machine using 3-dimensional $6 \times 6 \text{mm}^2$ macular volume scan mode (512 A scans per B scan; 128 horizontal B scans). The imaging was completed on undilated eyes in a dark room following other eye measurements [13]. The right eye was consistently imaged first, and the majority of individuals had imaging repeated in their left eyes [12].

The images were processed using the industry standard Topcon advanced boundary software (TABS) [14]. This software performs automated retinal layer segmentation. It calculated thickness values for each of the retinal layers averaged across the macular field, as well as in each of the subfields of the early treatment of diabetic retinopathy study (ETDRS) grid [15]. The ETDRS is a nine-segment grid arranged as a bullseye and is commonly used during clinical assessment of the macula including the PRCs (fig. 1B).

Quality Control of Genotypic and Phenotypic Data

Participants who were recommended for exclusion from genetic studies by the UK Biobank were removed from the dataset. The most densely populated well-mixed population was selected for using principal component analysis. Individuals within a defined euclidean distance of the mean of the selected population, as identified by comparison to the HapMap Phase III study [16] in PC1-PC2 space were selected. Individuals were further excluded if they were related to third degree or more [17].

In addition to the genotypic quality control, rigorous quality control was applied to the phenotypic data. Exclusion/inclusion criteria were applied to the OCT images and the quantitative measures derived from them utilising methods previously implemented in Patel *et al.* (2016) [18]. In line with this method all participants with an OCT image quality score <45 were removed from the study. Further, individuals with values within the poorest 20% of the population in each of the OCT segmentation indicators were removed. These segmentation indicators include: Inner limiting membrane (ILM) indicator, a measure of the minimum localised edge strength around the ILM boundary across the entire OCT scan. ILM indicator is indicative of blinks, severe signal fading, and segmentation errors; Valid count, used to identify significant clipping in the z-axis of the OCT scan; Minimum motion correlation, maximum motion delta and maximum

motion factor, all of which utilise the nerve fibre layer and total retinal thickness to calculate Pearson correlation and absolute differences between the thickness values from each set of consecutive B-scans. The lowest correlation and highest absolute difference in a scan define the resulting indicator values. These values identify blinks, eye motion artefacts and segmentation failures. It should be noted that the image quality score and segmentation indicators are often correlated with one another. Finally individuals with outlier values of refractive error were removed from the study. Outlier refractive error scores were defined as values lying outside one standard deviation of 1.5 times the inter-quartile range from the median. The final dataset included 31,135 individuals.

Genome-wide Association Studies

GWAS were implemented using an additive linear model in BGENIE [17]. The mean thickness of each component PRC layer across the ETDRS grid was used as the input phenotype (fig. 1C). Eye-specific covariates including image quality measures obtained from the OCT machine (listed above) and refractive error (calculated as $spherical\ error + 0.5 \times cylindrical\ error$) were regressed out of thickness values for the left and right eye separately before a mean was made across the two eyes. Covariates including age, weight, sex, height, OCT machine ID and the first 20 genotype PCs were used in the model. A genome-wide significance threshold of $P < 5 \times 10^{-8}$ was used. LD-score regression was implemented using LD SCorE v1.0 [19].

Associated variant discovery set

The summary statistics from the GWAS of the ONL, IS and OS were meta-analysed using MTAG [20]. The resulting lowest p-value of the three meta-analysed phenotypes was considered the meta p-value. The meta-analysed PRC results were filtered using GCTA Conditional and Joint Analysis (COJO) [21] to select for independent SNPs that were more than 10Mb apart. Further filtering was applied and loci within 1.5Mb of one another were labelled as being in the same locus as indicated in the results tables where loci considered to be within the same locus are shaded the same colour, alternating grey and white (table S3). A plot of a magnified locus of interest was generated using LocusZoom [22].

Exome analysis

We performed gene burden testing using the UK Biobank (UKBB) 200,000 whole exome release to search for genes that showed an increased level of rare loss of function (LoF) or rare missense variants that were predicated as deleterious and probably damaging. Briefly, we ran the ensemble variant effect predictor (VEP) [23] on the multi sample VCF from the 200K UKBB release to allow us to classify variants and assign their consequence. We defined high confidence LoF variants using the VEP plugin LOFTEE and selected missense variants using SIFT “deleterious” and Polyphen “probably_damaging” flags, all variants were filtered to have a minor allele frequency (MAF) of less than 1% prior to collapsing into gene based genotypes for burden testing. To define gene level genotypes we used the standard collapsing method where we considered all variants within the gene for each sample separately and defined zero, one and two (0,1,2) genotypes based on: zero (genotype 0) no rare variant of the given type present in the gene; one (genotype 1) more than zero rare variants of the given type present in the gene but all are in the heterozygous state; and two (genotype 2) if any of the rare variants of the given type where in the homozygous state. It is worth noting that by using this approach we do not account for compound heterozygous mutations or the overall variant load within individual genes but it does allow us to interrogate

potential rare variant associations to the trait of interest at the gene level. To perform the association testing we treated the gene level genotypes for rare LoF and potentially damaging missense variants as standard genotypes within a linear model with covariates against the OCT derived PRC layers. The covariates included within the models and the overall sample selection was exactly the same as for the common SNP GWAS analysis. A significance threshold of $P < 5 \times 10^{-5}$ was used.

Annotation of variants and geneset enrichment

Significant variants were manually annotated with associated gene and any prior ophthalmic or general phenotypic associations using ENSEMBL [24] and Open Targets Genetics platform [25]. Geneset and tissue enrichment analysis was conducted using DEPICT [26].

Comparison of Genetic Effect on Retinal Sub-fields

The foveal, intermediate and peripheral fields of the ETDRS grid were considered separately (fig. 2). A mean thickness of each of the PRC layers was calculated across each of these fields. A GWAS was then performed for each of these phenotypes. Eye specific covariates were regressed out of the individual eye measurements prior to a mean being made across left and right eyes, as described above. The same covariates were used in these GWAS as were in the simple phenotype GWAS. The GWAS were performed using BEGENIE [17].

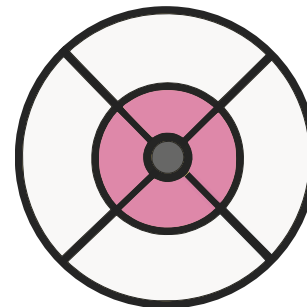


Fig 2. Comparison of concentric rings defined by the ETDRS grid. The macula divided into three concentric fields for comparison utilising the ETDRS grid. The peripheral field is shaded white, the intermediate field is shaded pink and the foveal field is shaded grey.

To compare the genetic effect of each SNP on the different subfields, each retinal layer was considered at a time. For each PRC layer, comparisons were made between the genetic effect on: the foveal field compared to the intermediate field; the foveal field compared to the peripheral field; and the intermediate field compared to the peripheral field. For each comparison, SNPs were selected that were significantly associated with either of the two phenotypes being considered. A z-score was calculated for each of the SNPs comparing the genetic effect size for the two phenotypes. The z-score was defined as:

$$Z = \frac{|\beta_0 - \beta_1|}{\sqrt{SE_0^2 + SE_1^2}}$$

P-values were calculated for each of the z-scores and SNPs selected that were significant following bonferroni correction. The list of SNPs was clumped into loci based on linkage disequilibrium values. Each variant was annotated with all SNPs with $r^2 > 0.05$ in a 1000kb window using PLINK and the locus with the lowest p-value in each window selected.

Visualisation of spatial genetic effect

A linear model was assessed of the effect of each of the loci identified as differentially affecting the concentric retinal fields on the thickness of each of the PRC layers in each of the nine segments in the ETDRS grid. The model included the same covariates as the GWAS of average retinal thickness and the effect size was plotted back into the ETDRS grid space.

Interaction models

Linear models were used to explore the presence of genetic interaction effecting the thickness of the three PRC layers. The same covariates were used as those used in the GWAS. Significance values were corrected for multiple testing using Benjamini and Hochberg correction and a false discovery threshold of < 0.15 was used.

Results

Initially we conducted three genome wide association studies (GWAS), one for the thickness of each component PRC layer - the ONL, IS and OS - averaged across both the ETDRS grid and across both left and right eyes (fig. 1C). This is analogous to many clinical uses of macular layer thicknesses. Quality control was applied to the OCT image data consistent with previous work [9,18] and we used a well established method to select the European-associated PCA cluster using genetic data, which aims to minimise variation in non-genetic factors and genetic factors (See Methods). The resulting subset of samples that passed both image and genetic filters comprised of 31,135 individuals (table S1). The three GWAS (one for each component layer of the PRC), each identified a number of associated loci using the established genome-wide significance level of $P < 5 \times 10^{-8}$ threshold. Following calculation of the linkage disequilibrium score for each of the three GWAS, there was minimal evidence for inflation due to residual population structure (fig. S1, table S2). SNP heritability of the thickness of each of the PRC layers was calculated: ONL $h^2=0.39$, IS $h^2=0.18$, and OS $h^2=0.21$. Unsurprisingly we observed numerous loci that were significantly associated with the thickness of more than one of the PRC layers, and so we meta-analysed results using MTAG [20]. Following selection of independent loci using COJO [21], there were 111 loci significantly associated with the meta-analysed PRC layers' thickness (Figure fig. 3, table S3 and table S4).

We immediately noticed that many of these loci were close to well known genes associated with rare ocular diseases (fig. 4 and table S5). 17 of the 111 loci overlap with a known rare retinal disease locus, which is highly unlikely to occur by chance ($P < 2.2 \times 10^{-16}$ Hypergeometric distribution).

We further leveraged the initial release of the UK Biobank exome dataset of 247,000 individuals, complementing the common variation GWAS with a rare variation gene burden test on the same phenotypes. We considered both strict loss of function mutations and overall missense mutations as two separate tests applied to each layer. Although there were no strong rare variant hits, setting a more liberal significance threshold ($P < 5 \times 10^{-5}$) - consistent with other exome wide burden tests - we found 10 significant loci (table S6, fig. S2). Three of these loci overlap with rare eye disease, again unlikely to have been observed by chance ($P=2.65 \times 10^{-6}$ by hypergeometric distribution).

Overall between rare and common discovery we have found over 100 loci associated with PRC thickness in some manner, and these continuous quantitative phenotype associations have significant overlap to known rare ocular disease genes.

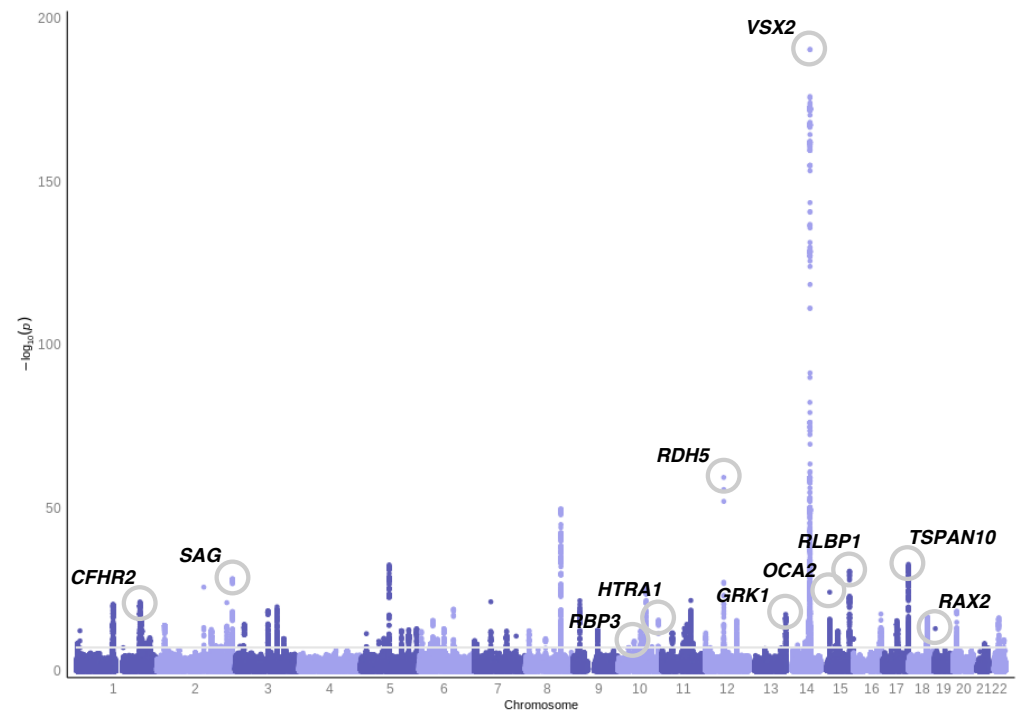


Fig 3. Genome-wide association study of photoreceptor cell layer thickness phenotypes. Manhattan plot of the photoreceptor cell layer thickness phenotype GWAS p-values. These result from meta-analysis using MTAG [20] of the summary statistics from GWAS of the thickness of the outer nuclear layer (ONL), inner segment (IS) and outer segment (OS). Variants are considered significantly associated if they reach genome wide significance ($P < 5 \times 10^{-8}$). Loci of interest, selected through manual labelling by ophthalmic experts, are circled and labelled.

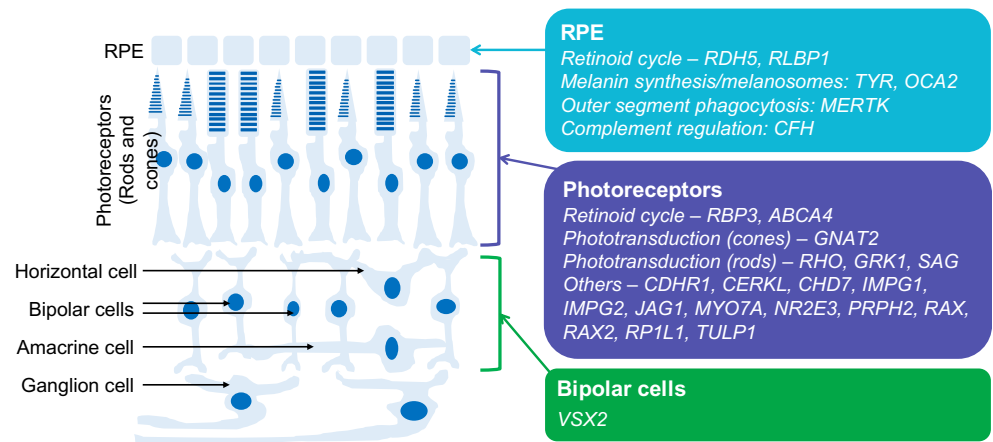


Fig 4. Schematic of retina showing main cell types with sites of expression (in mature human retina) of many of the genes associated with rare monogenic ocular disease found during genetic discovery (table S5). Some genes are also expressed significantly in other cell types not shown (e.g. *RLBP1* is expressed also in Muller cells). Also, some genes (including those not shown) have a wider role in development, but expression is more restricted in adults (e.g. *VSX2* is expressed in retinal progenitor cells in development, but mainly in bipolar cells in the mature retina).

Selected Loci of Interest

Of these genetic variants, the locus with the smallest p-value and with a reasonably large effect size for a single locus was *VSX2*. *VSX2* is a homeobox transcription factor that has been found expressed in the developing retina of humans, mice and zebrafish [27]. The gene is known to have an important role in ocular size, with pathogenic variants leading to microphthalmia [27]. This locus showed allelic heterogeneity in the GWAS results with the most significant genetic variant being rs1972565 ($P = 5.23 \times 10^{-191}$) whilst COJO analysis retained 4 other SNPs across the *VSX2* locus. In addition, there are SNPs in nearby genes which could be long range regulatory SNPs for *VSX2* rather than the closest genes we have assigned this to (fig. 5). Interestingly in previous work we identified genetic variants in neighbouring loci that had a statistically significant effect on the thickness of the inner retinal layers [9]. All this evidence points towards the *VSX2* locus having multiple alleles which affect different aspects of eye development.

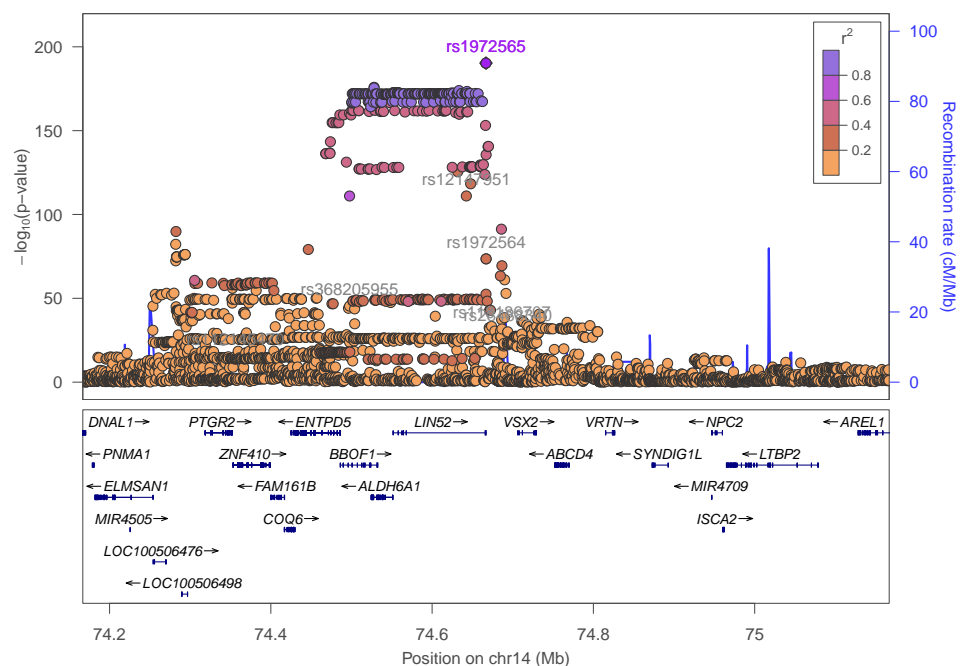


Fig 5. Magnification of the *VSX2* locus. Association of the locus on chromosome 14 centred on the genetic variant rs1972565 (highlighted in purple). Other genetic variants found significantly associated with PRC thickness are labelled in grey.

Further there were several loci found associated with PRC layer thickness that are known to be involved in the retinoid cycle. The retinoid or visual cycle refers to the recycling of chromophore: photons of light isomerise 11-*cis* retinal to all-*trans* retinal in the photoreceptor outer segments; to be converted back to 11-*cis* retinal, a multi-stage process is entailed, which includes transport to the retinal pigment epithelium and then back to the photoreceptor [28]. *RDH5*, *RLBP1* and *RBP3*, all found associated with PRC layer thickness, each have a known role in the retinoid cycle and are associated with rare inherited retinal diseases. *RDH5* (rs3138142, $P = 5.58 \times 10^{-60}$) encodes 11-*cis* retinol dehydrogenase, an enzyme responsible for conversion of 11-*cis* retinol to 11-*cis* retinal. The specific SNP in *RDH5* (rs3138142, $P = 5.58 \times 10^{-60}$) has previous associations with a number of ophthalmic phenotypes including the age one started

wearing glasses, cataract and myopia. Pathogenic variants in this gene are known to cause fundus albipunctatus, a retinal dystrophy and form of night blindness that primarily affects the rods [29,30]. *RLBP1* (rs3825991, $P = 2.70 \times 10^{-31}$) encodes the cellular retinaldehyde binding protein, a transporter of 11-*cis* retinal [31,32]. Mutations in this gene lead to a number of different retinal dystrophies [33]. *RBP3* (rs111245635, $P = 8.41 \times 10^{-10}$) encodes the interphotoreceptor retinoid-binding protein which has a role in transporting retinoids between the RPE and the photoreceptor cells [34]. Additionally, rare variants within *RBP3* cause recessive retinal dystrophy and high myopia [35]. Much of the retinoid cycle occurs in the supporting RPE layer, for example *RDH5* is almost exclusively expressed in this layer [36], showing that one does not need gene expression in a cell type to impact its structure.

Two loci, *SAG* (rs7564805, $P = 6.16 \times 10^{-29}$) and *GRK1* (rs9796234, $P = 4.69 \times 10^{-18}$), were found associated with PRC layer thickness and these genes have known involvement in Oguchi disease. Oguchi disease is a rare autosomal recessive disease. Features include the Mizuo-Nakamura phenomenon, a golden retinal sheen and night-blindness [37]. *SAG* encodes arrestin and *GRK1* encodes rhodopsin kinase; both proteins are involved in shut-off of activated rhodopsin, enabling termination of the light response. When these proteins are dysfunctional, rhodopsin continues to activate the phototransduction cascade, shutting off the cyclic nucleotide-gated current, hyperpolarising the rods, and rendering them electrically unresponsive to further light photons. Thus patients primarily experience night blindness in this disorder. Studies have also found changes in the microstructure of the retinal layers in Oguchi disease patients [38,39]. The presence of common variation in these genes suggests that there might be functional differences in rod physiological due to genetics present at the population level.

Further, several variants were found in the large heterogenous *NPLOC4-TSPAN10* locus, and both rare and common variants were discovered in the *OCA2* locus. Variants in these loci have previously been found associated with foveal structure [9] suggesting that overall retinal development has an impact on the PRC layer. Additionally the *NPLOC4-TSPAN10* locus is associated with strabismus, the abnormal alignment of the eyes [40]. Strabismus is known to be caused by defects in the extraocular muscles, cranial nerves, refractive error and visual cortex processing. Our finding suggests there may be a role of retinal structure in strabismus which warrants further investigation utilising appropriate clinical datasets.

We also note that several loci significantly associated with the PRC layer thicknesses had prior associations to AMD. These included *CFHR2* (rs410895, $P=8.19 \times 10^{-22}$), *HTRA1* (rs60401382, $P=2.43 \times 10^{-16}$) and *RAX2* (rs76076446, $P=1.07 \times 10^{-13}$). AMD is a disease characterised by the atrophy of PRCs caused by the accumulation of lipid deposits in the RPE. Extensive recent work has previously been completed to study the relationship between PRC thickness and AMD [41,42].

The discovery of loci associated with PRC thickness at genes encoding proteins involved in phototransduction, generating the photoreceptor electrical response to light, is of interest. These include *GNAT2*, *SAG*, *GRK1* and *RHO*. This suggests there is a shared importance of these genes between phototransduction and structure. It may warrant further investigation into the relationship between the structure and function of these cells and these variants might provide interesting genetic instruments for the integration of the physiological process of light transduction with other features.

To further explore the biological pathways underlying PRC morphology, we used DEPICT [26] to perform gene set and tissue enrichment analysis. When applied to the loci associated with PRC thickness, numerous genesets reached statistical significance following false discovery rate (FDR) correction (table S7). These include ocular-associated genesets such as *abnormal lens morphology*, *microphthalmia*,

disorganized retinal layers and *abnormal ocular fundus morphology* amongst others. Additionally, tissue enrichment analysis of the loci associated with PRC thickness resulted in significant associations with *retina* and *eye* tissue (table S8).

Additionally, there were a number of genes identified in the gene-burden test analysis with interesting prior associations. These include *OCA2*, also significantly associated in our GWAS analysis, which has a prior association to oculocutaneous albinism. Individuals with this condition are characterised by foveal hypoplasia, the absence of the formation of the foveal pit. Further, three genes, *ABCA4*, *MYO7A* and *NR2E3*, are shown to have an association to PRC thickness and have a prior association with retinal dystrophies. *ABCA4* encodes ATP-binding cassette sub-family A member 4, a protein expressed almost exclusively in the PRCs. It is responsible for mediation of all-trans-retinal aldehyde across the PRC membrane, clearing it from the retina following phototransduction. *ABCA4* is the gene most frequently implicated in monogenic retinal dystrophies [5,43]. Biallelic pathogenic variants are the most common cause of juvenile macular degeneration (Stargardt disease) and can also give rise to a cone-rod dystrophy. *MYO7A* encodes myosin VIIA, a protein found in inner ear and retina. Within the PRCs, this protein helps regulate transport of opsins, light-sensitive proteins required for vision. Mutations in *MYO7A* are known to cause Type 1 Usher Syndrome, a condition characterised by deafness and retinal degeneration [44]. *NR2E3* encodes a nuclear receptor transcription factor that activates rod development and represses cone development [45]. Mutations in this gene are also associated with retinitis pigmentosa in addition to enhanced S-cone syndrome [46].

Fine grained topography of genetic variation

In addition to the clinically utilised measure of the mean PRC thickness taken across the ETDRS grid, TABS outputs the thickness of each of the PRC layers within each of the nine ETDRS subsections. To capitalise on this increased dimensionality of data, we explored how genetic variation affects PRC morphology in the different areas of the ETDRS segmentation grid. We chose to consider the macular field split into three concentric fields which align with the topography of the valley-like macula (fig. 2). A mean thickness across each of these concentric fields - the foveal, intermediate and peripheral fields - was taken for each of the PRC layers. These phenotypes were used as an input to GWAS and the SNPs which passed the significance threshold of 5×10^{-8} were taken forward for further analysis. Z-score analysis was applied to the resulting effect size to identify loci with significantly different effect on thickness of the different concentric fields of each PRC layer. Numerous (32) loci were found in each layer that affect the thickness of the concentric fields differentially (fig. 6, fig. S3).

The locus showing the most significant difference in effect on the thickness of the ONL across the concentric fields was *RREB1* (rs75757892) which had a differential effect on the foveal field (effect size=-1.12) compared to both the intermediate field (effect size=-0.55) and peripheral field (effect size=-0.20). *RREB1* encodes a zinc finger transcription factor, the Ras-responsive element binding protein 1 [47]. Genetic variants at *RREB1* have prior associations to various ocular phenotypes including the age one starts wearing glasses and spherical power.

The locus showing the most significantly different genetic effect on the IS thickness across the macula was *TMEM106B* (rs13237518) which had a significant difference between the foveal field (effect size=-0.23), and the peripheral field (effect size=-0.02). *TMEM106B* is known to be involved in frontotemporal lobar degeneration, a neurodegenerative disease [48]. There is growing interest in the use of OCT derived retinal thickness measures as biomarkers for neurodegenerative diseases [49,50] making this finding of potential interest.

The locus with the most significantly different genetic effect on the thickness of the

OS was *RDH5* also found in the initial meta-GWAS. *RDH5* (rs3138142) shows a significantly different effect on the thickness in the peripheral field (effect size=0.81) compared to both the foveal field (effect size=1.37) and the intermediate field (effect size=1.28). As described above *RDH5* encodes 11-*cis* retinol dehydrogenase, an enzyme that is part of the retinoid cycle. It has been previously associated with the retinal dystrophy, fundus albipunctatus.

Notably several further loci were discovered to differentially affect the concentric fields of the retina that had prior associations with retinal dystrophies. These include *MERTK* (rs869016) which shows a significant difference of effect across the concentric fields of the OS. It has a significantly larger effect size on the fovea (effect size=-0.31) as compared to the peripheral field (effect size=0.02). *MERTK* encodes MER proto-oncogene, tyrosine kinase, a transmembrane protein localised to the RPE. *MERTK* has a known role in the phagocytosis of the OS by the RPE. Mutations in *MERTK* have been associated with retinitis pigmentosa and early onset retinal dystrophies [51].

Additionally *CDHR1* (rs55798570) shows a significantly different effect size on the thickness of the IS in the foveal field (effect size=0.13) compared to both the intermediate field (effect size=0.002) and the peripheral field (effect size=-0.06). *CDHR1* encodes cadherin-related family member 1, a cell adhesion protein that localises to the junction of the IS and OS. Genetic variants in *CDHR1* have been associated with a number of inherited retinal dystrophies including retinitis pigmentosa and cone-rod dystrophy [52].

Further *RAX2* (rs76076446), shows a different effect on the thickness of the IS at the fovea (effect size=0.31) compared to the peripheral field (effect size=-0.09). *RAX2* encodes retina and anterior neural fold homeobox 2, which has a known role in eye development. Pathological variants in this locus are known to cause cone and rod dysfunction and retinitis pigmentosa, a rod-cone disease [53].

Each of these retinal dystrophies have distinct and sometimes opposing spatio-temporal patterns in which they affect the rods and cones. Some dystrophies, including retinitis pigmentosa, affect the rods first, with the cones affected later. Patients have problems with night vision, then peripheral vision, and finally central vision. Fundus albipunctatus also affects rod function, whilst cones are usually spared. Others such as cone-rod dystrophy affect the cones first and the rods afterwards. Cones are found at the highest density at the fovea, whilst rod density peaks more peripherally. There appears to be a parallel between the spatial genetic effects of these loci on thickness of the PRC and the organisation of PRCs affected by the diseases associated with these loci.

Genetic Interactions

As there are both clear common biological pathways associated with multiple discovered variants, and overlaps with known rare disease loci we wanted to explore whether genetic interactions were affecting the retinal phenotype. Genetic interactions of common variation are challenging to discover and characterise due to the large space of possible interactions. To restrict our space we considered interactions in the following categories: (1) Interactions of the developmentally important *VSX2* locus internally and with all other common genetic variants; (2) Interactions between the Retinoid cycle loci; (3) Interactions of the Oguchi syndrome loci; (4) Interaction of all loci with genetically defined sex; and (5) Interactions between rare burden levels in genes and nearby common SNPs.

Overall we do not find widespread interaction terms that would pass multiple testing criteria. There was no statistically significant interaction term between the genetic variants with prior association to Oguchi disease, or between those with a prior

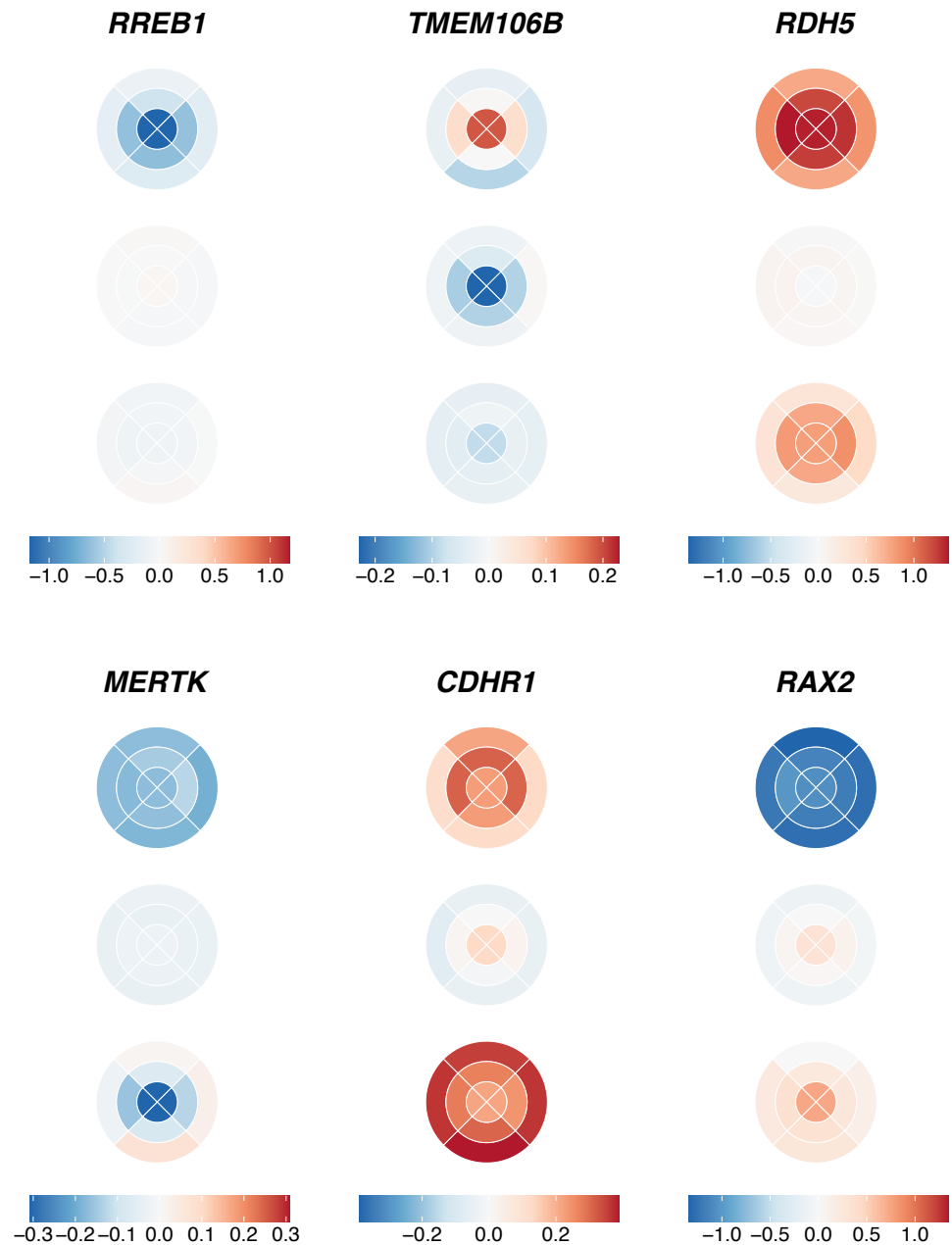


Fig 6. Effect size of selected SNPs on ETDRS grid The figure shows the effect size of the SNPs (shown by a blue-red gradient) with differential effect on the concentric fields of the retina, on the nine different segments of the ETDRS grid across the three PRC layers listed from top to bottom: ONL, IS and OS. Six loci are visualised: *RREB1* (rs75757892), *TMEM106B* (rs13237518), *RDH5* (rs3138142), *MERTK* (rs869016), *CDHR1* (rs55798570), and *RAX2* (rs76076446). Effect sizes are scaled for each genetic locus individually.

association with the retinoid cycle. Additionally, there was no evidence of an interaction between any of the 111 identified loci and genetically defined sex. There was no evidence for interactions between rare burden levels in genes and nearby common SNPs; however this analysis was limited by the sample size of individuals with heterozygous alternative allelic states. Expansion of this analysis in a cohort containing a higher proportion of individuals with rare disease phenotypes would have more power to identify interactions.

However, following Benjamini and Hochberg correction for multiple testing, and using a False Discovery threshold level of < 0.15 , four variants show an interaction with the lead *VSX2* SNP, rs1972565 in relation to their effect on ONL thickness. Two of the four variants (rs112145470 and rs28488340) are within the same locus as *VSX2*, consistent with the already noted allelic heterogeneity at this locus. The other two loci are *DYNLRB2* (rs7206532) and *PRPH2* (rs375435). *DYNLRB2* is expressed in retinal Muller cells and astrocytes, and encodes dyenin light chain roadblock type 2. Mutations in this gene are associated with deafness and hepatocellular cancer. *PRPH2* encodes peripherin 2 which is localised to the photoreceptors. Mutations in this gene are known to result in forms of retinal dystrophy and macular degeneration [54]. Upon stratification of the population by their genotype at *VSX2* and *PRPH2*, a change in ONL thickness can be observed, specifically between *PRPH2* homozygous reference and homozygous alternative genotype in those with the *VSX2* homozygous reference genotype (fig. 7, fig. S4). In individuals with *PRPH2* homozygous reference, a thinner ONL is found in the superior segments of the macula, and thicker ONL in the inferior segments. In individuals with *PRPH2* homozygous alternative, the inverse pattern is seen. This is of particular interest as there is often a difference in PRC degeneration across the macula equator in retinal dystrophies. *PRPH2* has a documented spectrum of penetrance and associated disease phenotypes [55, 56]. This finding suggests one of the possible mechanisms by which the effects of variants at the *PRPH2* locus are modified is via the genotype at the *VSX2* locus.

Discussion

Here we have performed the largest and most detailed GWAS and rare variation association of PRC layer thickness to date, leveraging the high-dimensional spatial resolution available within retinal OCT. We initially explored a simple phenotype of the mean thickness of each of the PRC layers - the ONL, IS, OS - across the entire macula field as defined by the ETDRS grid. These phenotypes are advantageous in that they are aligned with those used in clinical practice. Using these phenotypes, we identified 111 independent loci significantly associated with one or more of the component PRC layers following GWAS meta analysis and 10 loci associated with rare variation following gene burden testing. Many of the loci identified here had prior associations to ocular phenotypes and the loci collectively were enriched for known rare ocular diseases.

The collection of rare disease loci discovered in this study of common, physiologically healthy individuals without obvious eye diseases shows the continuum between common and rare variation, and rare variation which leads to disease. In this study we explicitly looked for interactions between common variation at different loci and common and rare variation at the same loci. We found several relatively weak interactions between a SNP near the well known eye development gene, *VSX2*, and two SNPs within this locus as well as two SNPs near *PRPH2* and *DYNLRB2*. No evidence was found for an interaction between common and rare genetic variants but this was partially due to limitations of the dataset and its absence of adequate numbers of individuals with rare variation and subsequent lack of statistical power.

Genetic discovery also found sets of loci associated with PRC thickness with prior associations to different ocular phenotypes. Four loci (*GNAT2*, *SAG*, *GRK1* and *RHO*)

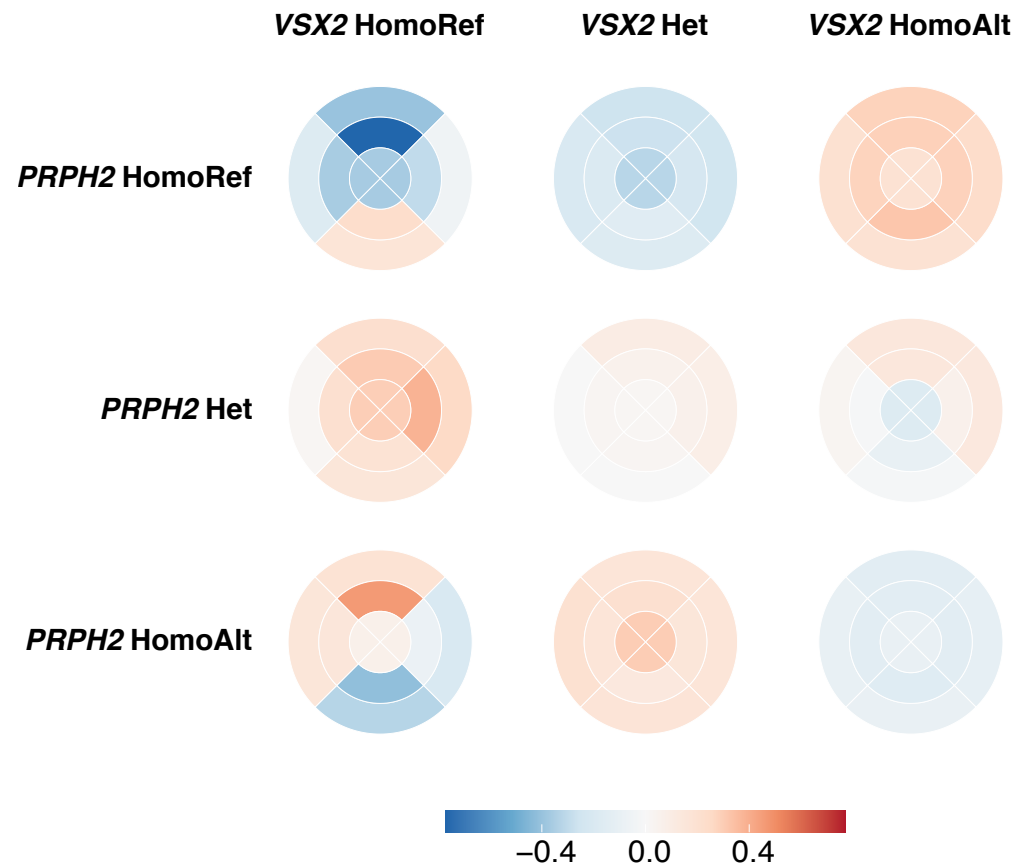


Fig 7. Normalised thickness of ONL stratified by *VSX2* and *PRPH2* genotype. The mean thickness of the ONL at each of the nine segments of the ETDRS grid across individuals stratified by their genotype at *VSX2* and *PRPH2*. The thickness is mean normalised per *VSX2* genotype.

have a prior association to phototransduction, the generation of an electrical response to light in the PRC. Further three variants were found in or near genes (*RDH5*, *RLBP1* and *RBP3*) with prior associations to the retinoid cycle, the process by which the chromophore is regenerated following photoisomerisation by light. In both cases, this finding suggests a relationship between the form and function of these cells which may warrant further investigation. Whilst it might be intuitive that genes encoding structural and matrix proteins are associated with photoreceptor layer thicknesses, it is interesting that genes encoding proteins involved in bringing about or shaping the photoreceptor electrical light response to light are also implicated, potentially suggesting a role for visual signalling in development or maintenance of outer retinal structure.

There were several loci associated with specific disease. For example both *SAG* and *GRK1* in addition to an association with PRC thickness have a known involvement in Oguchi disease, a rare autosomal eye condition which causes visual impairment. As well as the overlap between rare eye genetic disease and these common variants affecting retinal structure, there are some interesting, less expected findings. For example, three loci - *MYEOV* (rs10737153), *TNS1* (rs201030469) and *FGFR2* (rs17102399) - have impacts on both PRC layer thickness and risk of diagnosis for breast cancer. Additionally *TMEM106B*, which had a particularly notable spatial genetic effect, has a known association to a form of dementia. In both cases, the link between morphology and disease suggests the possibility of using OCT derived PRC morphology measures as biomarkers for complex diseases in the future. Additional datasets enriched for individuals with these diseases with OCT data will be required to further explore these concepts.

This study has offered the ability to study the genetics underlying complex retinal structures. Whilst OCT does not directly offer single-cell resolution, the quantitative values extracted from the images in the photoreceptor layer describe a single cell layer and capture variation in sub-cellular structures. It is interesting to note that some of the strong hits have gene expression in a different cell type. For example *RDH5* which is strongly associated with thickness of all three PRC layers is expressed in the RPE [57]. Therefore we are identifying genetic variation impacting sub-cellular morphology in a between cell type manner, highlighting the complex route between genetic variation, gene function and ultimate physiological differences. Imaging offers a methodology for interrogating such processes at a high-dimensional scale in a non-invasive manner and the protocol used here could be applied to other organs of the human body.

Data Availability

The genetic and phenotypic UK Biobank data are available upon application to the UK Biobank.

Acknowledgments

The authors are extremely grateful for the selfless participation of individuals in the UK Biobank used in this study and the staff managing these cohorts. HC has received support from EMBL and is supported by Novo Nordisk Foundation (grants NNF17OC0027594 and NNF14CC0001). APK is supported by a UKRI Future Leaders Fellowship and an Alcon Young Investigator Award. TWF and EB are supported by EMBL. OAM is supported by the Wellcome Trust (206619/Z/17/Z). The UK Biobank Eye and Vision Consortium members are: Naomi Allen, Tariq Aslam, Denize Atan, Sarah Barman, Jenny Barrett, Paul Bishop, Graeme Black, Tasanee Braithwaite, Roxana Carare, Usha Chakravarthy, Michelle Chan, Sharon Chua, Alexander Day,

Parul Desai, Bal Dhillon, Andrew Dick, Alexander Doney, Cathy Egan, Sarah Ennis, 529
 Paul Foster, Marcus Fruttiger, John Gallacher, David Garway-Heath, Jane Gibson, 530
 Jeremy Guggenheim, Chris Hammond, Alison Hardcastle, Simon Harding, Ruth Hogg, 531
 Pirro Hysi, Pearse Keane, Peng Tee Khaw, Anthony Khawaja, Gerassimos Lascaratos, 532
 Thomas Littlejohns, Andrew Lotery, Phil Luthert, Tom MacGillivray, Sarah Mackie, 533
 Bernadette McGuinness, Gareth McKay, Martin McKibbin, Tony Moore, James Morgan, 534
 Richard Oram, Eoin O’Sullivan, Chris Owen, Praveen Patel, Euan Paterson, Tunde 535
 Peto, Axel Petzold, Nikolas Pontikos, Jugnoo Rahi, Alicja Rudnicka, Naveed Sattar, Jay 536
 Self, Panagiotis Sergouniotis, Sobha Sivaprasad, David Steel, Irene Stratton, Nicholas 537
 Strouthidis, Cathie Sudlow, Zihan Sun, Robyn Tapp, Dhanes Thomas, Emanuele 538
 Trucco, Adnan Tufail, Ananth Viswanathan, Veronique Vitart, Mike Weedon, Katie 539
 Williams, Cathy Williams, Jayne Woodside, Max Yates, Jennifer Yip, Yalin Zheng. 540

Author Contribution 541

HC conceived the analysis, performed the analysis and wrote the paper. TWF 542
 performed analysis and wrote the paper. PJP, APK and ARW provided advice on 543
 analysis. OAM performed analysis and oversaw the work. EB conceived the analysis, 544
 wrote the manuscript and oversaw the work. All authors reviewed the final manuscript. 545

Competing Interests 546

APK has acted as a consultant to Abbvie, Aerie, Google Health, Novartis, Reichert, 547
 Santen and Thea. 548

References

1. Tick S, Rossant F, Ghorbel I, Gaudric A, Sahel JA, Chaumet-Riffaud P, et al. Foveal Shape and Structure in a Normal Population. *Investigative Ophthalmology & Visual Science*. 2011;52(8):5105–5110. doi:10.1167/IOVS.10-7005.
2. Chopra R, Wagner SK, Keane PA. Optical coherence tomography in the 2020s—outside the eye clinic. *Eye* 2020 35:1. 2020;35(1):236–243. doi:10.1038/s41433-020-01263-6.
3. Fritsche LG, Igl W, Bailey JNC, Grassmann F, Sengupta S, Bragg-Gresham JL, et al. A large genome-wide association study of age-related macular degeneration highlights contributions of rare and common variants. *Nature Genetics*. 2016;48(2):134–143. doi:10.1038/ng.3448.
4. Chakravarthy U, Evans J, Rosenfeld PJ. Age related macular degeneration. *BMJ*. 2010;340(7745):526–530. doi:10.1136/BMJ.C981.
5. Pontikos N, Arno G, Jurkute N, Schiff E, Ba-Abbad R, Malka S, et al. Genetic Basis of Inherited Retinal Disease in a Molecularly Characterized Cohort of More Than 3000 Families from the United Kingdom. *Ophthalmology*. 2020;127(10):1384–1394. doi:10.1016/J.OPHTHA.2020.04.008.
6. Khawaja AP, Chua S, Hysi PG, Georgoulas S, Currant H, Fitzgerald TW, et al. Comparison of Associations with Different Macular Inner Retinal Thickness Parameters in a Large Cohort: The UK Biobank. *Ophthalmology*. 2020;127(1). doi:10.1016/j.ophtha.2019.08.015.

7. Pilat AV, Proudlock FA, Mohammad S, Gottlob I. Normal macular structure measured with optical coherence tomography across ethnicity. *British Journal of Ophthalmology*. 2014;98(7):941–945. doi:10.1136/bjophthalmol-2013-303119.
8. Gao XR, Huang H, Kim H. Genome-wide association analyses identify 139 loci associated with macular thickness in the UK Biobank cohort. *Human Molecular Genetics*. 2019;28(7):1162–1172. doi:10.1093/hmg/ddy422.
9. Currant H, Hysi P, Fitzgerald TW, Gharahkhani P, Bonnemaier PWM, Senabouth A, et al. Genetic variation affects morphological retinal phenotypes extracted from UK Biobank optical coherence tomography images. *PLOS Genetics*. 2021;17(5):e1009497. doi:10.1371/journal.pgen.1009497.
10. Elliott P, Biobank oboU, Peakman TC, Biobank oboU. The UK Biobank sample handling and storage protocol for the collection, processing and archiving of human blood and urine. *International Journal of Epidemiology*. 2008;37(2):234–244. doi:10.1093/IJE/DYM276.
11. Cumberland PM, Rahi JS, Consortium ftUBE, Vision. Visual Function, Social Position, and Health and Life Chances: The UK Biobank Study. *JAMA Ophthalmology*. 2016;134(9):959–966. doi:10.1001/JAMAOPHTHALMOL.2016.1778.
12. Keane PA, Grossi CM, Foster PJ, Yang Q, Reisman CA, Chan K, et al. Optical Coherence Tomography in the UK Biobank Study – Rapid Automated Analysis of Retinal Thickness for Large Population-Based Studies. *PLOS ONE*. 2016;11(10):e0164095. doi:10.1371/JOURNAL.PONE.0164095.
13. Khawaja AP, Bailey JNC, Wareham NJ, Scott RA, Simcoe M, Igo RP, et al. Genome-wide analyses identify 68 new loci associated with intraocular pressure and improve risk prediction for primary open-angle glaucoma. *Nature Genetics*. 2018;50(6):778–782. doi:10.1038/s41588-018-0126-8.
14. Yang Q, Reisman CA, Wang Z, Fukuma Y, Hangai M, Yoshimura N, et al. Automated layer segmentation of macular OCT images using dual-scale gradient information. *Optics express*. 2010;18(20):21293. doi:10.1364/OE.18.021293.
15. Camparini M, Cassinari P, Ferrigno L, Macaluso C. ETDRS-fast: implementing psychophysical adaptive methods to standardized visual acuity measurement with ETDRS charts. *Investigative Ophthalmology & Visual Science*. 2001;42(6):1226–1231.
16. Altshuler DM, Gibbs RA, Peltonen L, Schaffner SF, Yu F, Dermitzakis E, et al. Integrating common and rare genetic variation in diverse human populations. *Nature*. 2010;467(7311):52–58. doi:10.1038/nature09298.
17. Bycroft C, Freeman C, Petkova D, Band G, Elliott LT, Sharp K, et al. The UK Biobank resource with deep phenotyping and genomic data. *Nature*. 2018;562(7726):203–209. doi:10.1038/s41586-018-0579-z.
18. Patel PJ, Foster PJ, Grossi CM, Keane PA, Ko F, Lotery A, et al. Spectral-Domain Optical Coherence Tomography Imaging in 67 321 Adults: Associations with Macular Thickness in the UK Biobank Study. *Ophthalmology*. 2016;123(4):829–840. doi:10.1016/J.OPHTHA.2015.11.009.

19. Bulik-Sullivan BK, Loh PR, Finucane HK, Ripke S, Yang J, Patterson N, et al. LD Score regression distinguishes confounding from polygenicity in genome-wide association studies. *Nature Genetics* 2015 47:3. 2015;47(3):291–295. doi:10.1038/ng.3211.
20. Turley P, Walters RK, Maghzian O, Okbay A, Lee JJ, Fontana MA, et al. Multi-trait analysis of genome-wide association summary statistics using MTAG. *Nature Genetics*. 2018;50(2):229–237. doi:10.1038/s41588-017-0009-4.
21. Yang J, Ferreira T, Morris AP, Medland SE, Madden PAF, Heath AC, et al. Conditional and joint multiple-SNP analysis of GWAS summary statistics identifies additional variants influencing complex traits. *Nature Genetics*. 2012;44(4):369–375. doi:10.1038/ng.2213.
22. Pruim RJ, Welch RP, Sanna S, Teslovich TM, Chines PS, Gliedt TP, et al. LocusZoom: regional visualization of genome-wide association scan results. *Bioinformatics* (Oxford, England). 2010;26(18):2336–2337. doi:10.1093/BIOINFORMATICS/BTQ419.
23. McLaren W, Gil L, Hunt SE, Riat HS, Ritchie GRS, Thormann A, et al. The Ensembl Variant Effect Predictor. *Genome Biology*. 2016;17(1):122. doi:10.1186/s13059-016-0974-4.
24. Howe KL, Achuthan P, Allen J, Allen J, Alvarez-Jarreta J, Ridwan Amode M, et al. Ensembl 2021. *Nucleic Acids Research*. 2021;49(D1):D884–D891. doi:10.1093/nar/gkaa942.
25. Ghoussaini M, Mountjoy E, Carmona M, Peat G, Schmidt EM, Hercules A, et al. Open Targets Genetics: Systematic identification of trait-associated genes using large-scale genetics and functional genomics. *Nucleic Acids Research*. 2021;49(D1):D1311–D1320. doi:10.1093/nar/gkaa840.
26. Pers TH, Karjalainen JM, Chan Y, Westra HJ, Wood AR, Yang J, et al. Biological interpretation of genome-wide association studies using predicted gene functions. *Nature Communications*. 2015;6(1):1–9. doi:10.1038/ncomms6890.
27. Reis LM, Khan A, Kariminejad A, Ebadi F, Tyler RC, Semina EV. VSX2 mutations in autosomal recessive microphthalmia. *Molecular Vision*. 2011;17:2527–2532.
28. Tsin A, Betts-Obregon B, Grigsby J. Visual cycle proteins: Structure, function, and roles in human retinal disease. *Journal of Biological Chemistry*. 2018;293(34):13016–13021. doi:10.1074/jbc.AW118.003228.
29. Gonzalez-Fernandez F, Kurz D, Bao Y, Newman S, Conway BP, Young JE, et al. 11-cis Retinol dehydrogenase mutations as a major cause of the congenital night-blindness disorder known as fundus albipunctatus. *Molecular Vision*. 1999;5(41):41–41.
30. Rotenstreich Y, Harats D, Shaish A, Pras E, Belkin M. Treatment of a retinal dystrophy, fundus albipunctatus, with oral 9-cis- β -carotene. *British Journal of Ophthalmology*. 2010;94(5):616–621. doi:10.1136/bjo.2009.167049.
31. Saari JC, Nawrot M, Kennedy BN, Garwin GG, Hurley JB, Huang J, et al. Visual cycle impairment in cellular retinaldehyde binding protein (CRALBP) knockout mice results in delayed dark adaptation. *Neuron*. 2001;29(3):739–748. doi:10.1016/S0896-6273(01)00248-3.

32. Wu Z, Hasan A, Liu T, Teller DC, Crabb JW. Identification of CRALBP ligand interactions by photoaffinity labeling, hydrogen/deuterium exchange, and structural modeling. *Journal of Biological Chemistry*. 2004;279(26):27357–27364. doi:10.1074/jbc.M401960200.
33. Hipp S, Zobor G, Glöckle N, Mohr J, Kohl S, Zrenner E, et al. Phenotype variations of retinal dystrophies caused by mutations in the RLBP1 gene. *Acta Ophthalmologica*. 2015;93(4):e281–e286. doi:10.1111/aos.12573.
34. den Hollander AI, McGee TL, Ziviello C, Banfi S, Dryja TP, Gonzalez-Fernandez F, et al. A homozygous missense mutation in the IRBP gene (RBP3) associated with autosomal recessive retinitis pigmentosa. *Investigative Ophthalmology and Visual Science*. 2009;50(4):1864–1872. doi:10.1167/iovs.08-2497.
35. Arno G, Hull S, Robson AG, Holder GE, Cheetham ME, Webster AR, et al. Lack of Interphotoreceptor Retinoid Binding Protein Caused by Homozygous Mutation of RBP3 Is Associated With High Myopia and Retinal Dystrophy. *Investigative Ophthalmology & Visual Science*. 2015;56(4):2358–2365. doi:10.1167/IOVS.15-16520.
36. Xie Y, Gonome T, Yamauchi K, Maeda-Monai N, Tanabu R, Ishiguro Si, et al. A spectral-domain optical coherence tomographic analysis of Rdh5^{-/-} mice retina. *PLOS ONE*. 2020;15(4):e0231220. doi:10.1371/JOURNAL.PONE.0231220.
37. Nishiguchi KM, Ikeda Y, Fujita K, Kunikata H, Akiho M, Hashimoto K, et al. Phenotypic Features of Oguchi Disease and Retinitis Pigmentosa in Patients with S-Antigen Mutations: A Long-Term Follow-up Study. *Ophthalmology*. 2019;126(11):1557–1566. doi:10.1016/J.OPHTHA.2019.05.027.
38. Hayashi T, Tsuzuranuki S, Kozaki K, Urashima M, Tsuneoka H. Macular dysfunction in Oguchi disease with the frequent mutation 1147delA in the SAG gene. *Ophthalmic Research*. 2011;46(4):175–180. doi:10.1159/000325024.
39. Hashimoto H, Kishi S. Shortening of the rod outer segment in Oguchi disease. *Graefes Archive for Clinical and Experimental Ophthalmology*. 2009;247(11):1561–1563. doi:10.1007/S00417-009-1114-6/FIGURES/2.
40. Plotnikov D, Shah RL, Rodrigues JN, Cumberland PM, Rahi JS, Hysi PG, et al. A commonly occurring genetic variant within the NPLOC4–TSPAN10–PDE6G gene cluster is associated with the risk of strabismus. *Human Genetics* 2019 138:7. 2019;138(7):723–737. doi:10.1007/S00439-019-02022-8.
41. Kaye RA, Patasova K, Patel PJ, Hysi P, Lotery AJ, Patel PJ, et al. Macular thickness varies with age-related macular degeneration genetic risk variants in the UK Biobank cohort. *Scientific Reports* 2021 11:1. 2021;11(1):1–11. doi:10.1038/s41598-021-02631-2.
42. Zekavat SM, Sekimitsu S, Ye Y, Raghu V, Zhao H, Elze T, et al. Photoreceptor layer thinning is an early biomarker for age-related macular degeneration: Epidemiological and genetic evidence from UK Biobank optical coherence tomography data. *Ophthalmology*. 2022;doi:10.1016/J.OPHTHA.2022.02.001.
43. Stone EM, Andorf JL, Whitmore SS, DeLuca AP, Giacalone JC, Streb LM, et al. Clinically Focused Molecular Investigation of 1000 Consecutive Families with Inherited Retinal Disease. *Ophthalmology*. 2017;124(9):1314–1331. doi:10.1016/J.OPHTHA.2017.04.008.

44. Cheng L, Yu H, Jiang Y, He J, Pu S, Li X, et al. Identification of a novel MYO7A mutation in Usher syndrome type 1. *Oncotarget*. 2018;9(2):2295. doi:10.18632/ONCOTARGET.23408.
45. Peng GH, Ahmad O, Ahmad F, Liu J, Chen S. The photoreceptor-specific nuclear receptor Nr2e3 interacts with Crx and exerts opposing effects on the transcription of rod versus cone genes. *Human molecular genetics*. 2005;14(6):747–764. doi:10.1093/HMG/DDI070.
46. Li S, Datta S, Brabbit E, Love Z, Woytowicz V, Flattery K, et al. Nr2e3 is a genetic modifier that rescues retinal degeneration and promotes homeostasis in multiple models of retinitis pigmentosa. *Gene Therapy* 2020 28:5. 2020;28(5):223–241. doi:10.1038/s41434-020-0134-z.
47. Kent OA, Saha M, Coyaud E, Burston HE, Law N, Dadson K, et al. Haploinsufficiency of RREB1 causes a Noonan-like RASopathy via epigenetic reprogramming of RAS-MAPK pathway genes. *Nature Communications* 2020 11:1. 2020;11(1):1–12. doi:10.1038/s41467-020-18483-9.
48. Harding SR, Bocchetta M, Gordon E, Cash DM, Cardoso MJ, Druyeh R, et al. The TMEM106B risk allele is associated with lower cortical volumes in a clinically diagnosed frontotemporal dementia cohort. *Journal of Neurology, Neurosurgery & Psychiatry*. 2017;88(11):997–998. doi:10.1136/JNNP-2017-315641.
49. Van De Kreeke JA, Nguyen HT, Konijnenberg E, Tomassen J, Den Braber A, Ten Kate M, et al. Optical coherence tomography angiography in preclinical Alzheimer's disease. *British Journal of Ophthalmology*. 2020;104(2):157–161. doi:10.1136/BJOPHTHALMOL-2019-314127.
50. Chan VTT, Sun Z, Tang S, Chen LJ, Wong A, Tham CC, et al. Spectral-Domain OCT Measurements in Alzheimer's Disease: A Systematic Review and Meta-analysis. *Ophthalmology*. 2019;126(4):497–510. doi:10.1016/J.OPHTHA.2018.08.009.
51. Evans DR, Green JS, Johnson GJ, Schwartzentruber J, Majewski J, Beaulieu CL, et al. Novel 25 kb Deletion of MERTK Causes Retinitis Pigmentosa With Severe Progression. *Investigative Ophthalmology & Visual Science*. 2017;58(3):1736–1742. doi:10.1167/IOVS.16-20864.
52. Stingl K, Mayer AK, Llavona P, Mulahasanovic L, Rudolph G, Jacobson SG, et al. CDHR1 mutations in retinal dystrophies. *Scientific Reports* 2017 7:1. 2017;7(1):1–11. doi:10.1038/s41598-017-07117-8.
53. Van de Sompele S, Smith C, Karali M, Corton M, Van Schil K, Peelman F, et al. Biallelic sequence and structural variants in RAX2 are a novel cause for autosomal recessive inherited retinal disease. *Genetics in Medicine* 2018 21:6. 2018;21(6):1319–1329. doi:10.1038/s41436-018-0345-5.
54. Conley SM, Naash MI. Gene Therapy for PRPH2-Associated Ocular Disease: Challenges and Prospects. *Cold Spring Harbor Perspectives in Medicine*. 2014;4(11). doi:10.1101/CSHPERSPECT.A017376.
55. Boon CJF, den Hollander AI, Hoyng CB, Cremers FPM, Klevering BJ, Keunen JEE. The spectrum of retinal dystrophies caused by mutations in the peripherin/RDS gene. *Progress in Retinal and Eye Research*. 2008;27(2):213–235. doi:10.1016/J.PRETEYERES.2008.01.002.

56. Michaelides M, Holder GE, Bradshaw K, Hunt DM, Moore AT. Cone-rod dystrophy, intrafamilial variability, and incomplete penetrance associated with the R172W mutation in the peripherin/RDS gene. *Ophthalmology*. 2005;112(9):1592–1598. doi:10.1016/J.OPHTHA.2005.04.004.
57. Wen B, Li S, Li H, Chen Y, Ma X, Wang J, et al. Microphthalmia-associated transcription factor regulates the visual cycle genes Rlbp1 and Rdh5 in the retinal pigment epithelium. *Scientific Reports* 2016 6:1. 2016;6(1):1–9. doi:10.1038/srep21208.

Supporting information

Table S1. Comparison of biological characteristics between whole UK Biobank population with OCT data (n = 67,321), the group that passes our quality control criteria (n = 31,135), and the group that fails (n = 36,186). Results are presented as mean \pm standard deviation.

	Total OCT Population	Pass filter	Fail filter
Height (cm)	168.68 \pm 9.25	169.43 \pm 9.15	168.03 \pm 9.29
Age (years)	57 \pm 8	57 \pm 8	57 \pm 8
Weight (Kg)	78.12 \pm 16.02	78.47 \pm 15.82	77.82 \pm 16.17
Sex (m/f)	29,713/34,929	14,696/16,439	15,017/18,490
Refractive Error Left (Dioptres)	-0.32 \pm 2.73	0.23 \pm 1.49	-0.80 \pm 3.41
Refractive Error Right (Dioptres)	-0.38 \pm 2.73	0.18 \pm 1.48	-0.87 \pm 3.40

Table S2. Linkage score disequilibrium analysis results. Linkage score disequilibrium metrics for the three GWAS of the photoreceptor layers following analysis using LDSC [19]. Metrics include lambda genomic control (GC), linkage disequilibrium score (LDSC) intercept and LDSC ratio.

GWAS phenotype	lambda GC	LDSC intercept	LDSC ratio
ONL	1.15	1.04	0.13
IS	1.07	1	<0
OS	1.09	1.02	0.15

Table S3. 111 SNPs significantly associated ($P < 5 \times 10^{-8}$) with the thickness of one or more of the component photoreceptor cells (PRCs).

Each SNP is annotated with the associated gene and any prior associations to ocular or non-ocular phenotypes. Variants considered to be representative of a single locus, examples of allelic heterogeneity, are highlighted in the same colour alternating white and grey. Full results including effect size, effect allele specification and standard error are available in Supplementary Table S4.

SNP	Chr	P-value	Associated Gene	Ocular Phenotypes	Non-ocular Phenotypes
rs112248193	1	2.73E-09	<i>LRRC47</i>		High light scatter reticulocyte count
rs2128416	1	4.83E-13	<i>CASZ1</i>		Amlodipine, High blood pressure, Hypertension
rs11587687	1	5.02E-09	<i>GNAT2</i>		Frequency of tiredness/lethargy
rs3790612	1	2.60E-15	<i>ST7L</i>		Blood pressure, High blood pressure, Platelet distribution width
rs72683442	1	4.13E-21	<i>SLC16A1</i>	Spherical power	Birth weight
rs410895	1	8.19E-22	<i>CFHR2</i>	Macular degeneration	
rs6427827	1	2.50E-16	<i>ZNF281</i>	Age started wearing glasses, Spherical power	Urinary albumin excretion
rs11577827	1	2.77E-13	<i>KDM5B</i>		
rs919655	1	2.36E-09	<i>PROX1-AS1</i>		Mean spheroid cell volume, Oily fish intake
rs12140498	1	3.14E-09	<i>LINC02257</i>		Arm fat percentage, Colon cancer
rs6426584	1	7.03E-11	<i>CDC42BPA</i>		Impedance of arms, Neutrophil traits

Table S3. continued

rs7594221	2	1.07E-14	<i>ATAD2B</i>		Forced vital capacity, Height, Intelligence, Lymphocyte volume, Mean spheroid cell volume, Platelet traits, Reticulocyte traits
rs116350483	2	2.10E-26	<i>LINC01412</i>		Particulate matter air pollution
rs80265589	2	1.86E-13	<i>STK39</i>		Impedance of arm
rs28416292	2	1.78E-08	<i>CERKL</i>		
rs58172089	2	2.74E-08	<i>PLCL1</i>		Arm fat, Body mass index, Impedance of body
rs3755152	2	4.39E-10	<i>MREG</i>		
rs148388367	2	1.20E-21	<i>MREG</i>		
rs201030469	2	6.58E-09	<i>TNSI</i>		Breast cancer
rs7564805	2	6.16E-29	<i>SAG</i>		Crohn's disease, Inflammatory Bowel Disease
rs34234056	3	2.37E-08	<i>LINC01267</i>		
rs11129176	3	1.53E-08	<i>RARB</i>	Optic disc area	Height, Red blood cell count
rs6775323	3	5.79E-15	<i>LINC02084</i>		
rs62282867	3	4.63E-19	<i>IMPG2</i>		Heel bone mineral density
rs111163508	3	2.28E-20	<i>RHO</i>		
rs7430585	3	1.26E-10	<i>TSC22D2</i>	Age started wearing glasses	
rs115237855	5	3.73E-12	<i>BASP1-AS1</i>		
rs78303234	5	3.32E-08	<i>BASP1</i>		
rs30373	5	7.70E-10	<i>LINC01948</i>	Macular thickness	
rs63338061	5	9.81E-11	<i>MAP1B</i>	Age started wearing glasses	
rs17421627	5	3.30E-33	<i>LINC00461</i>	Macular thickness, Retinal vascular caliber	Comparative height at age 10, Seen doctor for nerves, anxiety, tension or depression
rs62391700	5	5.05E-13	<i>LMNB1-DT</i>		Height, Multiple myeloma
rs1109114	5	2.65E-13	<i>AFAP1L1</i>		Body mass index, Forced expiratory volume, High blood pressure, Hearing difficulties, Hypertension
rs1438692	5	1.32E-11	<i>AFAP1L1</i>		Forced expiratory volume
rs6875105	5	1.39E-13	<i>BOD1</i>	Refractive error	
rs2326838	6	7.86E-13	<i>RREB1</i>	Age started wearing glasses, Spherical equivalent, Spherical power	Lymphocyte traits, White blood cell count
rs12192672	6	8.88E-10	<i>RREB1</i>		Haemoglobin traits, Hair/balding pattern, Height, Red blood cell traits
rs17507554	6	3.93E-09	<i>NEDD9</i>	Macular thickness	
rs6923949	6	4.22E-09	<i>TULP1</i>		Ankle spacing width, Anthropometric traits, Basal metabolic rates, Forced expiratory volume, White blood cell count
rs375435	6	3.56E-16	<i>PRPH2</i>		Neutrophil percentage
rs6910414	6	1.87E-10	<i>DST-AS1</i>		Haemoglobin concentration, Red blood cell count
rs947340	6	1.17E-13	<i>IMPG1</i>		
rs74526772	6	1.13E-19	<i>ATG5</i>		Asthma
rs9639276	7	4.74E-10	<i>SUN1</i>		Body mass index, Forced expiratory volume, Impedance of body

Table S3. continued

rs12531825	7	5.94E-09	<i>GLCCI1-DT</i>		Average total household income, Educational attainment, Forced expiratory volume, Height, Leg fat, Time spent watching TV
rs12719025	7	6.39E-22	<i>COBL</i>	Macular thickness, Refractive error, Spherical power, Strong/weak meridian	
rs111963714	7	5.96E-13	<i>PILRB</i>		Platelet traits
rs34926272	7	2.03E-11	<i>UBE2H</i>		
rs62490856	8	5.02E-13	<i>RP1L1</i>	Ocalt macular dystrophy, Strong meridian	Body mass index, Forced expiratory volume, Heel bone mineral density, Myeloid white blood cell count, Platelet distribution width, Red blood cell distribution width
rs61675430	8	1.30E-10	<i>CHD7</i>		Lymphocyte traits, Neutrophil traits, Potassium in urine
rs13263941	8	2.07E-50	<i>RSPO2</i>	Strong/weak meridian	Coffee intake, Hair colour
rs376067714	8	2.73E-24	<i>RSPO2</i>		
rs9298817	9	2.90E-22	<i>MIR31HG</i>	Strong meridian	Hypothyroidism
rs10781177	9	1.49E-08	<i>RORB</i>	Age started wearing glasses, Spherical power	
rs717299	9	3.80E-13	<i>RORB</i>		Impedance of arm
rs111245635	10	8.41E-10	<i>RBP3</i>	Age started wearing glasses, Retinitis pigmentosa, Strong/weak meridian	Soya milk
rs1947075	10	7.86E-10	<i>ARHGAP22</i>	Macular thickness	
rs7916697	10	3.80E-13	<i>ATOH7</i>	Cup-disc ratio, Optic cup area, Optic disc area, Optic disc radius	Anthropometric traits, Basal metabolic rate, Forced expiratory volume, Gastro-oesophageal reflux
rs11200922	10	1.62E-26	<i>CDHR1</i>	Age started wearing glasses, Hypermetropia, Spherical power	
rs34309160	10	3.34E-08	<i>GBF1</i>		
rs17102399	10	2.44E-08	<i>FGFR2</i>		Breast cancer
rs60401382	10	2.43E-16	<i>HTRA1</i>	Macular degeneration, Other retinal disorders	Anthropometric traits, Basal metabolic rate, Intelligence, Stroke
rs1016934	11	2.18E-12	<i>ELP4</i>	Strong meridian	Processed meat intake
rs618838	11	1.79E-09	<i>ACTN3</i>		Anthropometric traits, Impedance of body, Overall health rating, Red blood cell traits
rs116233906	11	9.33E-14	<i>SMIM38</i>		Heel bone mineral density
rs10737153	11	3.18E-09	<i>MYEOV</i>		Body mass, Breast cancer, Impedance of leg
rs12574286	11	5.77E-15	<i>GDPD4</i>		Hypertrophy of salivary gland, Platelet distribution width
rs1126809	11	2.56E-22	<i>TYR</i>	Eye colour, Foveal hypoplasia, Intraocular pressure, Ocular albinism, Oculocutaneous albinism, Optic disc size	Breast cancer, Hair colour, Hearing difficulties, Number of cancers, Skin cancer, Skin colour, Sunburn, Vitiligo
rs6483429	11	2.67E-09	<i>SES3</i>		Hair/balding pattern
rs2080402	12	2.21E-12	<i>SLC6A13</i>	Age started wearing glasses	Comparative size at age 10, Lifetime number of sexual partners

Table S3. continued

rs3138142	12	5.58E-60	<i>RDH5</i>	Age started wearing glasses, Cataract, Macular thickness, Myopia, Pigmentary retinal dystrophy, Refractive error, Spherical power	Atrial fibrillation
rs76629482	12	3.38E-16	<i>NTN4</i>		
rs9796234	13	4.69E-18	<i>GRK1</i>		
rs28468687	14	1.02E-08	<i>RALGAP1</i>		
rs1254260	14	1.18E-09	<i>LINC02322</i>	Age started wearing glasses, Glaucoma, Spherical power	Anthropometric traits, Basal metabolic rate, Forced expiratory volume, Heel bone mineral density, Impedance of legs, Menarche
rs1956524	14	2.13E-08	<i>RAD51B</i>		Asthma, Hand grip strength, Hayfever, allergic rhinitis or eczema, Male-pattern balding
rs10135971	14	4.47E-16	<i>ACTN1-AS1</i>	Macular degeneration, Spherical power	Exercises (swimming, cycling, keep fit, bowling), Forced vital capacity, Haematocrit percentage, Leg mass, Platelet traits, Pulse rate, Sensitivity/hurt feelings
rs112145470	14	4.81E-16	<i>ZNF410</i>		
rs368205955	14	4.13E-46	<i>BBOF1</i>		Red cell distribution width
rs12147951	14	8.89E-112	<i>VSX2</i>		
rs1972565	14	5.23E-191	<i>VSX2</i>		
rs1972564	14	2.93E-74	<i>VSX2</i>		
rs118186707	14	1.70E-32	<i>VSX2</i>		
rs28488340	14	9.02E-31	<i>VSX2</i>		
rs888413	14	1.92E-14	<i>YLPM1</i>		Body fat percentage, Depression, Fed-up feelings, Guilty feelings, Monocyte count, Mood swings, Nervous feelings, Neuroticism, Platelet count, Worrier/anxious feelings
rs1800407	15	7.58E-25	<i>OCA2</i>	Age started wearing glasses, Cataract, Central retinal arteriolar equivalent, Central retinal vein equivalent, Cylindrical power, Eye colour, Macular thickness, Oculocutaneous albinism	Age of first facial hair, Hair colour, Skin cancer, Skin colour, Sunburn, Tanning
rs1648303	15	2.72E-08	<i>DUOX1</i>		
rs10083695	15	8.00E-13	<i>WDR72</i>		Haematocrit, Red blood cell count
rs3825991	15	2.70E-31	<i>RLBP1</i>		Age at menopause
rs1372613	15	1.31E-10	<i>LINS1</i>		
rs7206532	16	1.86E-09	<i>DYNLRB2</i>	Spherical power	
rs142963458	16	3.58E-18	<i>MEAK7</i>	Macular thickness	
rs1049868	16	1.91E-09	<i>GSE1</i>		Platelet traits

Table S3. continued

rs62064364	17	4.11E-16	<i>LINC02210-CRHR1</i>	Macular thickness	Alcohol consumption, Average total household income, Cereal type, Forced vital capacity, Hair/balding pattern, Hand grip strength, Height, Mean platelet volume, Mean reticulocyte volume, Mean spheroid cell volume, Nap during day, Neuroticism, Oily fish intake, Plays computer games, Red blood cell traits, Relative age of first facial hair, White matter microstructure axial diffusivities
rs4794029	17	1.95E-13	<i>ABI3</i>	Spherical power	Angina, Body fat, Coronary artery disease, Eosinophil traits, Forced expiratory volume, Height, High blood pressure, Impedance of limbs
rs56737642	17	2.87E-11	<i>FAAP100</i>	Age started wearing glasses, Catatract, Logmar, Spherical power	Ankle spacing width, Hair colour, Skin colour, Tanning
rs61586425	17	4.78E-12	<i>NPLOC4</i>		
rs62075724	17	2.91E-12	<i>TSPAN10</i>	Amblyopia, Cylindrical power, Logmar, Myopia, Spherical power	Hair colour, Tanning
rs7405453	17	2.24E-33	<i>TSPAN10</i>	Age started wearing glasses, Amblyopia, Astigmatism, Cylindrical power, Intraocular pressure, Logmar, Macular thickness, Spherical power	Ankle spacing width, Hair colour, Tanning
rs4800994	18	7.83E-10	<i>TCF4</i>		Frequency of stair climbing, Hot drink temperature, Length of time at current address, Number of days worked >10 mins, Works dayshift
rs1517034	18	3.90E-16	<i>RAX</i>		Eotaxin levels
rs17696543	18	2.93E-17	<i>CPLX4</i>		
rs76076446	19	1.07E-13	<i>RAX2</i>	Age-related macular degeneration, Cone-rod dystrophy, Macular thickness, Retinal dystrophy	
rs1232603	20	4.80E-12	<i>JAG1</i>		Birth weight, Haematocrit percentage, Haemoglobin concentration, Heel bone mineral density, Impedance of limbs, Red blood cell count
rs6077977	20	4.98E-19	<i>JAG1</i>		Heel bone mineral density, Height
rs8132685	21	3.58E-09	<i>C21orf62</i>		
rs2032576	22	4.80E-08	<i>MIATNB</i>		
rs5752638	22	1.63E-16	<i>MN1</i>		Cereal intake, Eosinophil count, Mean reticulocyte volume, Platelet traits, Pulse rate, Red blood cell count
rs5763593	22	1.01E-10	<i>MTMR3</i>		
rs2073946	22	5.17E-17	<i>LIF-AS1</i>		Heel bone mineral density, Immature reticulocyte fraction

Table S3. continued

rs75159625	22	2.83E-10	WNT7B	Macular thickness, Spherical power, Strong/weak meridian	Anthropometric traits, Contracture of palmar fascia, Haematocrit percentage, Red blood cell count
------------	----	----------	-------	--	---

Table S4. Expanded results of photoreceptor layer thickness genome-wide association studies. Extended results of GWAS of the three photoreceptor cell layers, the outer nuclear layer (ONL), inner segment (IS) and outer segment (OS) following meta-analysis as well as the results selected by meta-analysis using MTAG, labelled MTAG. Each locus found significantly associated following meta-analysis is listed alongside the chromosome (Chr) and location (BP). The reference and alternative alleles are listed alongside the allele frequency (AF) of the alternative allele (A1). The effect size refers to the effect of having an additional copy of the A1 allele and the standard error (SE) is further listed.

SNP	Chr	BP	A1	A2	AF	MTAG effect size	ONL effect size	OS effect size	IS effect size	MTAG p-value	ONL p-value	OS p-value	IS p-value	MTAG SE	ONL SE	OS SE	IS SE
rs112248193	1	3718402	A	G	0.13	-0.09	-0.26	-0.02	-0.09	2.73E-09	5.43E-04	0.60	2.73E-09	0.02	0.07	0.05	0.02
rs2128416	1	10700448	C	T	0.15	-0.53	-0.53	-0.02	-0.06	4.83E-13	4.83E-13	0.63	1.99E-04	0.07	0.07	0.04	0.02
rs11587687	1	110147801	A	G	0.44	0.18	-0.08	0.18	0.01	5.02E-09	0.12	5.02E-09	0.30	0.03	0.05	0.03	0.01
rs3790612	1	113084146	A	G	0.26	-0.27	-0.08	-0.27	-0.01	2.60E-15	0.17	2.60E-15	0.55	0.03	0.06	0.03	0.01
rs72683442	1	113468825	C	T	0.22	-0.35	-0.20	-0.35	-0.02	4.13E-21	1.18E-03	4.13E-21	0.16	0.04	0.06	0.04	0.01
rs410895	1	196898226	C	T	0.55	0.30	0.06	0.30	-0.01	8.19E-22	0.23	8.19E-22	0.17	0.03	0.05	0.03	0.01
rs6427827	1	200398387	A	T	0.62	0.42	0.42	-0.04	0.05	2.50E-16	2.50E-16	0.22	2.23E-06	0.05	0.05	0.03	0.01
rs11577827	1	202798831	T	C	0.53	0.37	0.37	0.07	0.05	2.77E-13	2.77E-13	0.03	6.56E-06	0.05	0.05	0.03	0.01
rs919655	1	214157972	A	G	0.12	0.46	0.46	2.03E-03	0.08	2.36E-09	2.36E-09	0.97	4.00E-07	0.08	0.08	0.05	0.02
rs12140498	1	222098690	T	C	0.20	0.37	0.37	0.08	0.05	3.14E-09	3.14E-09	0.04	2.89E-05	0.06	0.06	0.04	0.01
rs6426584	1	227374949	T	A	0.34	0.07	0.28	-0.03	0.07	7.03E-11	1.62E-07	0.36	7.03E-11	0.01	0.05	0.03	0.01
rs7594221	2	24112724	A	T	0.76	0.28	0.23	0.28	0.03	1.07E-14	8.19E-05	1.07E-14	0.01	0.04	0.06	0.04	0.01
rs116350483	2	145338686	T	C	0.02	-2.11	-2.11	-0.16	-0.33	2.10E-26	2.10E-26	0.19	2.86E-15	0.20	0.20	0.12	0.04
rs80265589	2	169027979	A	T	0.27	-0.42	-0.42	-0.14	-0.06	1.86E-13	1.86E-13	2.80E-05	4.21E-08	0.06	0.06	0.03	0.01
rs28416292	2	182507470	A	T	0.15	0.08	0.34	-0.02	0.08	1.78E-08	1.61E-06	0.61	1.78E-08	0.01	0.07	0.04	0.01
rs58172089	2	198916926	A	G	0.17	0.23	-0.07	0.23	-0.03	2.74E-08	0.32	2.74E-08	0.03	0.04	0.07	0.04	0.01
rs3755152	2	216822197	G	A	0.89	-0.31	0.42	-0.31	0.05	4.39E-10	5.15E-07	4.39E-10	1.83E-03	0.05	0.08	0.05	0.02
rs148388367	2	216850944	A	T	0.04	-1.30	-1.30	0.56	-0.14	1.20E-21	1.20E-21	9.63E-12	1.18E-06	0.14	0.14	0.08	0.03
rs201030469	2	218321984	G	A	0.14	-0.42	-0.42	-0.01	-0.07	6.58E-09	6.58E-09	0.82	1.30E-05	0.07	0.07	0.04	0.02
rs7564805	2	234228946	G	A	0.05	-0.78	-0.07	-0.78	0.01	6.16E-29	0.52	6.16E-29	0.55	0.07	0.12	0.07	0.02
rs34234056	3	14418444	G	A	0.51	0.17	0.01	0.17	-1.87E-03	2.37E-08	0.78	2.37E-08	0.86	0.03	0.05	0.03	0.01
rs11129176	3	25049310	A	G	0.28	0.32	0.32	0.02	0.04	1.53E-08	1.53E-08	0.60	1.31E-04	0.06	0.06	0.03	0.01
rs6775323	3	27721085	T	G	0.20	0.49	0.49	-0.04	0.08	5.79E-15	5.79E-15	0.34	4.35E-09	0.06	0.06	0.04	0.01
rs62282867	3	100972078	A	G	0.79	0.34	-0.16	0.34	-1.98E-03	4.63E-19	0.01	4.63E-19	0.88	0.04	0.06	0.04	0.01
rs111163508	3	129235423	C	G	0.16	-0.39	0.23	-0.39	0.03	2.28E-20	9.22E-04	2.28E-20	0.03	0.04	0.07	0.04	0.01
rs7430585	3	150112041	A	G	0.76	0.23	0.10	0.23	-0.05	1.26E-10	0.09	1.26E-10	2.66E-05	0.04	0.06	0.04	0.01
rs115237855	5	17186336	A	G	0.03	-0.68	0.17	-0.68	0.03	3.73E-12	0.29	3.73E-12	0.31	0.10	0.16	0.10	0.03
rs78303234	5	17218432	G	C	0.12	-0.26	-0.10	-0.26	0.01	3.32E-08	0.21	3.32E-08	0.58	0.05	0.08	0.05	0.02
rs30373	5	55745334	G	C	0.37	0.32	0.32	0.11	0.04	7.70E-10	7.70E-10	3.86E-04	4.10E-05	0.05	0.05	0.03	0.01
rs63338061	5	71486228	T	C	0.36	0.07	0.31	-7.24E-05	0.07	9.81E-11	3.71E-09	0.99	9.81E-11	0.01	0.05	0.03	0.01
rs17421627	5	87847586	G	T	0.07	1.15	1.15	0.16	0.17	3.30E-33	3.30E-33	0.01	4.57E-17	0.10	0.10	0.06	0.02
rs62391700	5	126093395	C	T	0.20	-0.45	-0.45	-0.13	-0.03	5.05E-13	5.05E-13	7.46E-04	0.04	0.06	0.06	0.04	0.01
rs1109114	5	148615946	T	C	0.43	0.37	0.37	-0.04	0.07	2.65E-13	2.65E-13	0.23	1.28E-10	0.05	0.05	0.03	0.01
rs1438692	5	148659664	A	G	0.42	0.07	0.32	-0.01	0.07	1.32E-11	3.59E-10	0.75	1.32E-11	0.01	0.05	0.03	0.01
rs6875105	5	173054917	C	T	0.38	-0.38	-0.38	-0.03	-0.03	1.39E-13	1.39E-13	0.27	4.48E-03	0.05	0.05	0.03	0.01
rs2326838	6	6901663	A	G	0.36	-0.23	-0.07	-0.23	-1.50E-03	7.86E-13	0.18	7.86E-13	0.89	0.03	0.05	0.03	0.01
rs12192672	6	7229619	A	G	0.30	-0.34	-0.34	0.01	-0.04	8.88E-10	8.88E-10	0.76	1.13E-04	0.06	0.06	0.03	0.01
rs17507554	6	11394287	A	G	0.05	0.69	0.69	-0.11	0.10	3.93E-09	3.93E-09	0.14	4.14E-05	0.12	0.12	0.07	0.02
rs6923949	6	35496366	G	A	0.82	0.23	0.36	0.23	0.04	4.22E-09	4.95E-08	4.22E-09	9.96E-04	0.04	0.07	0.04	0.01
rs375435	6	42661404	C	T	0.57	-0.25	-0.06	-0.25	-0.01	3.56E-16	0.20	3.56E-16	0.62	0.03	0.05	0.03	0.01
rs6910414	6	56726737	G	A	0.18	0.42	0.42	-0.16	-0.01	1.87E-10	1.87E-10	7.37E-05	0.67	0.07	0.07	0.04	0.01
rs947340	6	76747944	C	A	0.70	-0.25	-0.05	-0.25	0.03	1.17E-13	0.34	1.17E-13	0.02	0.03	0.06	0.03	0.01
rs74526772	6	106515218	A	T	0.04	-1.25	-1.25	-0.01	-0.18	1.13E-19	1.13E-19	0.90	6.24E-10	0.14	0.14	0.08	0.03
rs9639276	7	867033	T	C	0.17	0.41	0.41	-0.01	0.08	4.74E-10	4.74E-10	0.75	3.79E-09	0.07	0.07	0.04	0.01
rs12531825	7	8005174	A	G	0.12	0.45	0.45	0.09	0.08	5.94E-09	5.94E-09	0.07	2.34E-06	0.08	0.08	0.05	0.02
rs12719025	7	51100190	G	A	0.46	0.49	0.49	-3.73E-03	0.07	6.39E-22	6.39E-22	0.90	1.33E-10	0.05	0.05	0.03	0.01
rs111963714	7	99948655	G	T	0.21	0.27	0.20	0.27	0.03	5.96E-13	1.54E-03	5.96E-13	0.05	0.04	0.06	0.04	0.01
rs34926272	7	129591807	C	G	0.03	-1.05	-1.05	-0.15	-0.18	2.03E-11	2.03E-11	0.11	4.44E-08	0.16	0.16	0.10	0.03
rs62490856	8	10469030	A	G	0.13	0.33	-0.09	0.33	0.04	5.02E-13	0.25	5.02E-13	0.01	0.05	0.08	0.05	0.02
rs61675430	8	61671071	A	G	0.20	-0.41	-0.41	-7.74E-04	-0.06	1.30E-10	1.30E-10	0.98	1.33E-05	0.06	0.06	0.04	0.01

Table S4. continued

rs13263941	8	109121945	C	T	0.26	0.86	0.86	0.15	0.12	2.07E-50	2.07E-50	1.72E-05	6.09E-24	0.06	0.06	0.04	0.01
rs376067714	8	109141863	G	A	0.18	0.77	0.77	0.06	0.11	2.73E-24	2.73E-24	0.17	4.14E-12	0.08	0.08	0.05	0.02
rs9298817	9	21576591	C	A	0.66	-0.51	-0.51	-0.04	-0.04	2.90E-22	2.90E-22	0.21	6.77E-04	0.05	0.05	0.03	0.01
rs10781177	9	76593011	T	C	0.42	-0.29	-0.29	-0.01	-0.05	1.49E-08	1.49E-08	0.64	1.12E-05	0.05	0.05	0.03	0.01
rs717299	9	77185933	G	A	0.45	0.37	0.37	0.06	0.04	3.80E-13	3.80E-13	0.04	9.57E-05	0.05	0.05	0.03	0.01
rs111245635	10	48389841	T	C	0.02	1.26	1.26	0.30	0.23	8.41E-10	8.41E-10	0.02	1.27E-07	0.21	0.21	0.12	0.04
rs1947075	10	49741135	T	C	0.64	-0.32	-0.32	-0.07	-0.05	7.86E-10	7.86E-10	0.04	3.66E-06	0.05	0.05	0.03	0.01
rs7916697	10	69991853	G	A	0.76	-0.43	-0.43	-0.14	-0.06	3.80E-13	3.80E-13	1.40E-04	1.51E-07	0.06	0.06	0.04	0.01
rs11200922	10	85961758	G	A	0.46	0.33	0.08	0.33	-0.03	1.62E-26	0.12	1.62E-26	0.01	0.03	0.05	0.03	0.01
rs34309160	10	104034550	T	C	0.07	-0.53	-0.53	-0.04	-0.06	3.34E-08	3.34E-08	0.55	0.01	0.10	0.10	0.06	0.02
rs17102399	10	123435963	A	G	0.05	0.67	0.67	-0.02	0.07	2.44E-08	2.44E-08	0.75	3.95E-03	0.12	0.12	0.07	0.03
rs60401382	10	124227624	T	C	0.23	-0.30	0.07	-0.30	0.03	2.43E-16	0.27	2.43E-16	0.01	0.04	0.06	0.04	0.01
rs1016934	11	31720621	G	A	0.30	-0.39	-0.39	0.02	-0.03	2.18E-12	2.18E-12	0.46	0.01	0.06	0.06	0.03	0.01
rs618838	11	66328719	C	T	0.55	0.06	0.19	0.03	0.06	1.79E-09	1.49E-04	0.28	1.79E-09	0.01	0.05	0.03	0.01
rs116233906	11	68968271	A	C	0.04	-0.94	-0.94	-0.04	-0.11	9.33E-14	9.33E-14	0.59	3.09E-05	0.13	0.13	0.08	0.03
rs10737153	11	69281829	C	A	0.57	-0.30	-0.30	-0.02	-0.03	3.18E-09	3.18E-09	0.48	3.00E-03	0.05	0.05	0.03	0.01
rs12574286	11	76937602	C	G	0.21	-0.29	0.01	-0.29	0.01	5.77E-15	0.93	5.77E-15	0.41	0.04	0.06	0.04	0.01
rs1126809	11	89017961	A	G	0.30	-0.32	0.20	-0.32	0.04	2.56E-22	2.49E-04	2.56E-22	1.04E-03	0.03	0.05	0.03	0.01
rs6483429	11	95239787	T	C	0.46	-0.30	-0.30	8.18E-04	-0.04	2.67E-09	2.67E-09	0.98	4.72E-04	0.05	0.05	0.03	0.01
rs2080402	12	345175	C	T	0.56	0.22	-0.13	0.22	-0.03	2.21E-12	0.01	2.21E-12	3.18E-03	0.03	0.05	0.03	0.01
rs3138142	12	56115585	T	C	0.24	0.96	0.96	0.48	0.10	5.58E-60	5.58E-60	5.01E-41	7.10E-17	0.06	0.06	0.04	0.01
rs76629482	12	96178789	G	C	0.18	-0.53	-0.53	-0.06	-0.07	3.38E-16	3.38E-16	0.151	3.69E-07	0.07	0.07	0.04	0.01
rs9796234	13	114323997	C	T	0.52	0.27	0.19	0.27	0.03	4.69E-18	1.57E-04	4.69E-18	3.13E-03	0.03	0.05	0.03	0.01
rs28468687	14	36026342	A	G	0.18	0.38	0.38	0.06	0.05	1.02E-08	1.02E-08	0.13	2.01E-04	0.07	0.07	0.04	0.01
rs1254260	14	60835737	A	G	0.29	-0.20	0.25	-0.20	-0.03	1.18E-09	7.86E-06	1.18E-09	0.01	0.03	0.06	0.03	0.01
rs1956524	14	68800393	A	G	0.64	0.29	0.29	0.02	0.04	2.13E-08	2.13E-08	0.59	1.09E-03	0.05	0.05	0.03	0.01
rs10135971	14	69517494	A	G	0.34	0.43	0.43	-0.02	0.03	4.47E-16	4.47E-16	0.45	0.01	0.05	0.05	0.03	0.01
rs112145470	14	74356090	A	G	0.03	1.34	1.34	0.09	0.14	4.81E-16	4.81E-16	0.40	3.64E-05	0.17	0.17	0.10	0.03
rs368205955	14	74497636	G	T	0.02	-3.19	-3.19	-0.24	-0.50	4.13E-46	4.13E-46	0.08	1.56E-26	0.22	0.22	0.14	0.05
rs12147951	14	74642451	C	A	0.07	-2.34	-2.34	-0.10	-0.38	8.89E-112	8.89E-112	0.13	4.78E-67	0.10	0.10	0.06	0.02
rs1972565	14	74666824	G	A	0.82	1.91	1.91	0.11	0.30	5.23E-191	5.23E-191	0.01	7.95E-106	0.06	0.06	0.04	0.01
rs1972564	14	74666944	T	C	0.48	1.03	1.03	-0.04	0.15	2.93E-74	2.93E-74	0.22	1.40E-37	0.06	0.06	0.03	0.01
rs118186707	14	74686575	A	G	0.03	1.77	1.77	0.03	0.27	1.70E-32	1.70E-32	0.74	5.61E-18	0.15	0.15	0.09	0.03
rs28488340	14	74693803	G	C	0.40	-0.59	-0.59	-0.05	-0.08	9.02E-31	9.02E-31	0.14	1.07E-13	0.05	0.05	0.03	0.01
rs888413	14	75267396	T	C	0.47	0.39	0.39	0.07	0.07	1.92E-14	1.92E-14	0.02	3.64E-10	0.05	0.05	0.03	0.01
rs1800407	15	28230318	T	C	0.08	0.57	-0.03	0.57	-0.02	7.58E-25	0.70246515	7.58E-25	0.34	0.06	0.09	0.06	0.02
rs1648303	15	45445692	G	A	0.57	-0.28	-0.28	-0.01	-0.04	2.72E-08	2.72E-08	0.66	8.32E-04	0.05	0.05	0.03	0.01
rs10083695	15	53987147	G	A	0.49	-0.36	-0.36	-0.06	-0.06	8.00E-13	8.00E-13	0.03	5.67E-09	0.05	0.05	0.03	0.01
rs3825991	15	89761664	A	C	0.47	0.36	0.05	0.36	-0.04	2.70E-31	0.29	2.70E-31	1.10E-04	0.03	0.05	0.03	0.01
rs1372613	15	101204835	T	C	0.30	0.35	0.35	0.02	0.06	1.31E-10	1.31E-10	0.63	2.60E-07	0.05	0.05	0.03	0.01
rs7206532	16	80490131	C	T	0.52	0.30	0.30	0.02	0.03	1.86E-09	1.86E-09	0.56	3.06E-03	0.05	0.05	0.03	0.01
rs142963458	16	84561361	T	C	0.04	-0.73	0.77	-0.73	0.13	3.58E-18	3.55E-08	3.58E-18	4.56E-06	0.08	0.14	0.08	0.03
rs1049868	16	85706633	C	T	0.29	-0.34	-0.34	0.02	-0.05	1.91E-09	1.91E-09	0.61	3.52E-05	0.06	0.06	0.03	0.01
rs62064364	17	43654468	T	C	0.22	0.50	0.50	0.02	0.07	4.11E-16	4.11E-16	0.65	1.71E-07	0.06	0.06	0.04	0.01
rs4794029	17	47280301	C	T	0.68	0.24	0.06	0.24	-0.04	1.95E-13	0.27	1.95E-13	1.28E-04	0.03	0.05	0.03	0.01
rs56737642	17	79515509	G	A	0.48	-0.34	-0.34	0.21	-0.06	2.87E-11	2.87E-11	4.64E-11	3.90E-08	0.05	0.05	0.03	0.01
rs61586425	17	79590835	A	C	0.09	-0.48	-0.14	-0.48	-3.22E-03	4.78E-12	0.22	4.78E-12	0.89	0.07	0.11	0.07	0.02
rs62075724	17	79611410	C	T	0.46	0.38	0.38	-0.21	0.07	2.91E-12	2.91E-12	1.12E-10	1.94E-09	0.05	0.05	0.03	0.01
rs7405453	17	79615572	G	A	0.65	-0.39	0.40	-0.39	0.07	2.24E-33	4.81E-14	2.24E-33	3.40E-10	0.03	0.05	0.03	0.01
rs4800994	18	53403850	T	C	0.19	0.08	0.31	-0.12	0.08	7.83E-10	1.33E-06	1.88E-03	7.83E-10	0.01	0.06	0.04	0.01
rs1517034	18	56937489	A	G	0.31	0.45	0.45	-1.38E-03	0.07	3.90E-16	3.90E-16	0.97	9.89E-11	0.05	0.05	0.03	0.01
rs17696543	18	56971398	T	C	0.18	-0.56	-0.56	4.79E-03	-0.09	2.93E-17	2.93E-17	0.90	2.62E-10	0.07	0.07	0.04	0.01
rs76076446	19	3771586	A	G	0.02	-1.25	-1.25	0.14	-0.15	1.07E-13	1.07E-13	0.19	2.19E-05	0.17	0.17	0.10	0.04
rs1232603	20	10612963	T	C	0.33	-0.23	-4.45E-03	-0.23	0.01	4.80E-12	0.93	4.80E-12	0.56	0.03	0.05	0.03	0.01
rs6077977	20	10930708	G	A	0.49	0.27	-0.09	0.27	-0.01	4.98E-19	0.08	4.98E-19	0.28	0.03	0.05	0.03	0.01
rs8132685	21	34220618	T	C	0.52	-0.30	-0.30	-0.02	-0.04	3.58E-09	3.58E-09	0.54	1.01E-04	0.05	0.05	0.03	0.01
rs2032576	22	27089655	T	G	0.56	-0.28	-0.28	0.03	-0.04	4.80E-08	4.80E-08	0.41	1.19E-04	0.05	0.05	0.03	0.01
rs5752638	22	28188203	C	T	0.22	-0.51	-0.51	-0.09	-0.07	1.63E-16	1.63E-16	0.02	2.89E-08	0.06	0.06	0.04	0.01
rs5763593	22	30302238	C	T	0.63	0.34	0.34	-0.01	0.06	1.01E-10	1.01E-10	0.74	3.12E-09	0.05	0.05	0.03	0.01
rs2073946	22	30619599	A	G	0.31	0.46	0.46	0.07	0.08	5.17E-17	5.17E-17	0.04	2.82E-11	0.06	0.06	0.03	0.01
rs75159625	22	46377008	G	T	0.31	0.34	0.34	0.05	0.05	2.83E-10	2.83E-10	0.15	5.33E-05	0.05	0.05	0.03	0.01

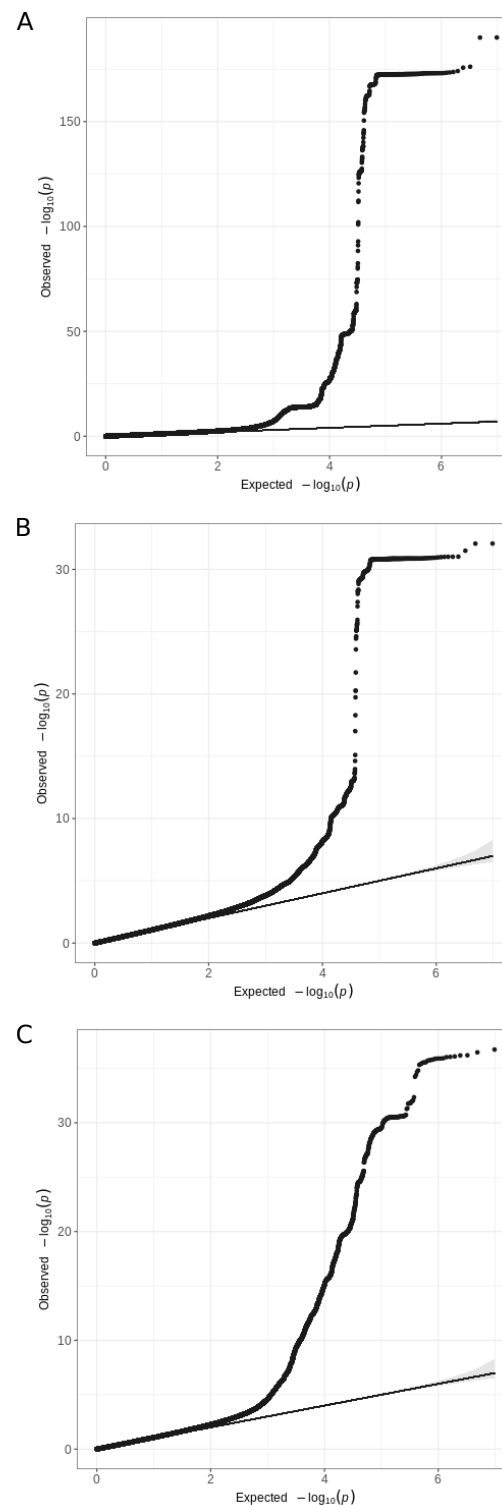


Fig S1. Quantile-quantile plots of outer retinal thickness genome-wide association studies (A) The quantile-quantile plot (qq-plot) for the GWAS of ONL thickness prior to meta-analysis (Lambda GC = 1.15, Intercept = 1.04, Ratio = 0.13). (B) The qq-plot for the GWAS of IS thickness prior to meta-analysis (Lambda GC = 1.07, Intercept = 1, Ratio < 0). (C) The qq-plot for the GWAS of OS thickness prior to meta-analysis (Lambda GC = 1.09, Intercept = 1.02, Ratio = 0.15).

Table S5. Selected rare monogenic ocular disease genes found to be associated with photoreceptor layer thicknesses in the present study.

Several genes are involved in bringing about or shaping the photoreceptors' electrical response to light (*RHO*, *GNAT2*, *SAG*, *GRK1*) or in recycling of the light-sensitive chromophore (*ABCA4*, *RLBP1*, *RBP3*, *RDH5*). Others are involved in maintaining outer retinal structure or in retinal and eye development. Superscript letters denote the relevant analyses in which the association was found: ^aGWAS; ^bdifferential association with ONL across concentric fields; ^cdifferential association with IS across concentric fields; ^ddifferential association with OS across concentric fields; ^eexome analysis.

Gene	Location	Encoded Protein and Function	Mendelian disease	Mode of inheritance
<i>Genes associated with rare monogenic retinal diseases</i>				
<i>CDHR1</i> ^{a,c}	10q23.1	Cadherin-related family member 1 (maintains rod and cone outer segment structure)	Cone-rod dystrophy; macular dystrophy	Recessive
<i>CERKL</i> ^a	2q31.3	Ceramide kinase-like protein (role in viability of cells with membranes rich in sphingolipids)	Rod-cone dystrophy; cone-rod dystrophy; widespread retinal degeneration	Recessive
<i>GNAT2</i> ^a	1p13.3	Cone-specific transducin (part of the phototransduction cascade in cone photoreceptors)	Achromatopsia (non-functioning cone photoreceptors)	Recessive
<i>GRK1</i> ^a	13q34	G-protein receptor kinase 1, rhodopsin kinase (phosphorylates activated rhodopsin to permit shut-off of the light response)	Oguchi disease, retinitis pigmentosa	Recessive
<i>IMPG1</i> ^a	6q14.1	Interphotoreceptor matrix proteoglycan 1 (role in retinal cell adhesion/ interphotoreceptor matrix)	Retinitis pigmentosa; vitelliform macular dystrophy	Dominant and recessive
<i>IMPG2</i> ^a	3q12.3	Interphotoreceptor matrix proteoglycan 2 (role in retinal cell adhesion/ interphotoreceptor matrix)	Retinitis pigmentosa; vitelliform macular dystrophy	Dominant and recessive
<i>JAG1</i> ^a	20p12.2	Jagged protein 1 (ligand for Notch proteins; function in cell-cell signalling)	Alagille syndrome	Dominant
<i>PRPH2</i> ^a	6p21.1	Peripherin-2 (important for rod and cone outer segment disc structure)	Macular pattern dystrophy; retinitis pigmentosa	Dominant and recessive
<i>RAX2</i> ^{a,c}	19p13.3	Retina and anterior neural fold homeobox 2 transcription factor	Retinitis pigmentosa; cone-rod dystrophy	Dominant and recessive
<i>RBP3</i> ^a	10q11.22	Retinol binding protein 3 (role in retinoid recycling)	Retinal dystrophy associated with high myopia	Recessive
<i>RDH5</i> ^{a,b,d}	14q24.1	Retinol dehydrogenase 5 (role in retinoid recycling)	Fundus albipunctatus, retinitis pigmentosa	Recessive
<i>RHO</i> ^a	3q22.1	Rhodopsin (forms visual pigment in rods)	Retinitis pigmentosa	Dominant and recessive
<i>RLBP1</i> ^a	15q26.1	Retinaldehyde-binding protein 1 (role in retinoid recycling)	Bothnia dystrophy, retinitis pigmentosa	Recessive
<i>RP1L1</i> ^a	15q26.1	Retinitis pigmentosa 1-like protein 1 (role in photoreceptor connecting cilia)	Occult macular dystrophy; retinitis pigmentosa	Dominant and recessive

Table S5. continued

<i>SAG</i> ^a	2q37.1	S-antigen, arrestin (binds activated rhodopsin to permit shut-off of the light response)	Oguchi disease, retinitis pigmentosa	Recessive and dominant
<i>TULP1</i> ^a	6p21.31	Tubby-like protein 1 (role in rhodopsin transport within photoreceptors)	Retinitis pigmentosa; Leber congenital amaurosis	Recessive
<i>CFH</i> ^d	1q31.3	Complement factor H (regulates alternative complement pathway)	Early onset macular drusen	Dominant
<i>MERTK</i> ^d	2q13	c-mer protooncogene receptor tyrosine kinase (loss of function leads to defective phagocytosis of photoreceptor outer segments by RPE)	Retinitis pigmentosa; early onset retinal dystrophy	Recessive
<i>ABCA4</i> ^e	1p22.1	ATP-binding cassette transporter A4 (functions as a flippase for N-retinylidene-phosphatidylethanolamine; aids clearing of all-trans retinaldehyde)	Stargardt disease macular dystrophy; cone-rod dystrophy	Recessive
<i>NR2E3</i> ^e	15q23	Nuclear receptor subfamily 2 group E3 (transcription factor, role in rod photoreceptor development; loss of function leads to excess of S-cones)	Enhanced S-cone syndrome, Goldmann-Faver syndrome, retinitis pigmentosa	Recessive and dominant
<i>MYO7A</i> ^e	11q13.5	Myosin VIIA (motor protein functions in transport of opsin in photoreceptors and melanosomes in RPE)	Type 1 Usher syndrome (retinitis pigmentosa and deafness)	Recessive
<i>Genes associated with oculocutaneous albinism (and foveal hypoplasia)</i>				
<i>OCA2</i> ^{a,e}	15q12-15q13.1	Oculocutaneous albinism 2 melanosomal transmembrane protein (protein regulates pH of melanosomes)	Oculocutaneous albinism	Recessive
<i>TYR</i> ^a	11q14.3	Tyrosinase (role in melanin synthesis)	Oculocutaneous albinism	Recessive
<i>Genes associated with rare monogenic ocular maldevelopment (including microphthalmia)</i>				
<i>VSX2</i> ^{a,b}	14q24.3	Visual system homeobox 2 (role in eye development)	Microphthalmia	Recessive
<i>PITX2</i> ^e	4q25	Paired-like homeodomain transcription factor 2 (role in eye development)	Anterior segment dysgenesis; microphthalmia	Dominant
<i>ATOH7</i> ^a	10q21.3	Atonal basic helix-loop-helix transcription factor 7 (role in eye development)	Persistent primary hypoplastic vitreous; ocular maldevelopment, including microphthalmia	Recessive
<i>CHD7</i> ^a	8q12.2	Chromodomain helicase DNA-binding protein 7 (role in control of neurocrest gene expression and in regulation of cell motility)	CHARGE syndrome	Dominant
<i>RARB</i> ^a	3p24.2	Retinoic acid receptor beta (role in eye and other organ development)	Microphthalmia, syndromic	Dominant and recessive
<i>RAX</i> ^a	18q21.32	Retina and anterior neural fold homeobox (role in eye development)	Microphthalmia	Recessive

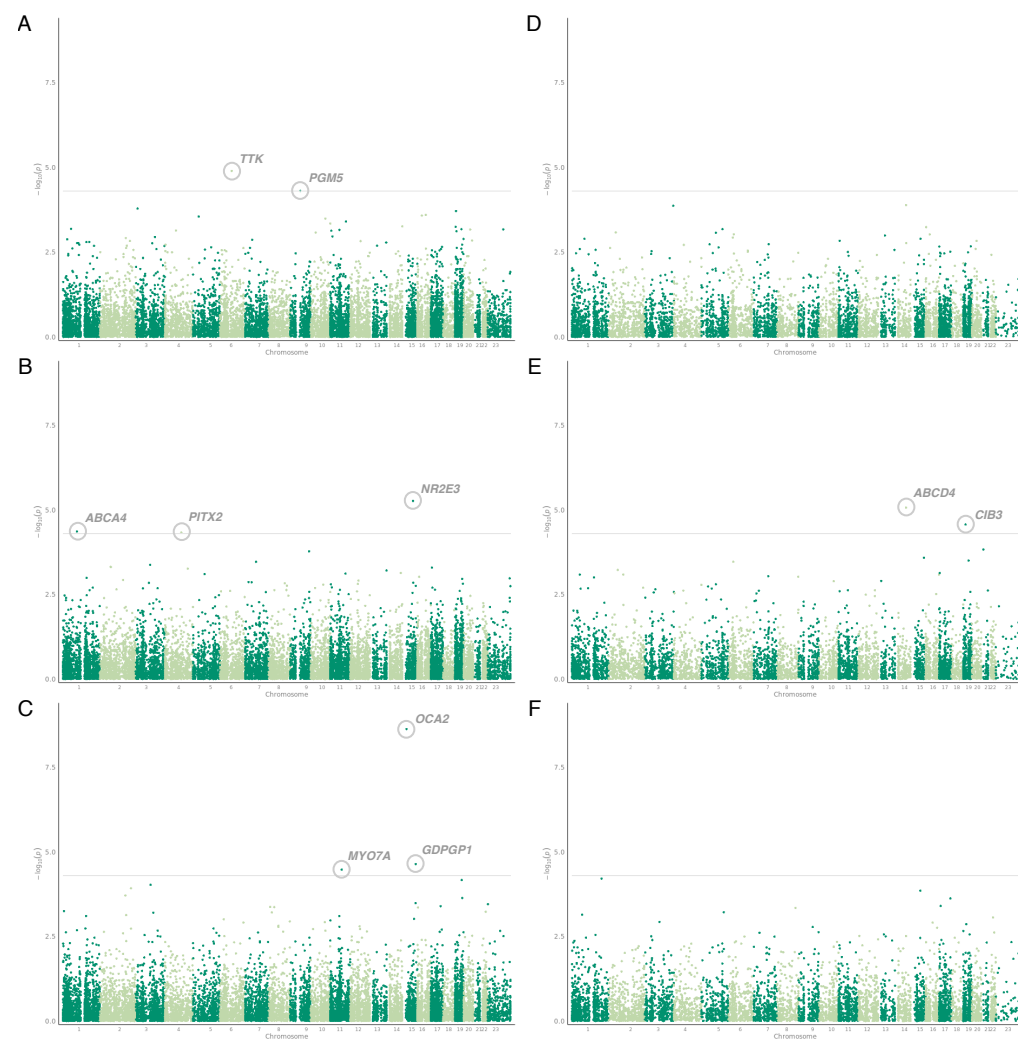


Fig S2. Exome-wide loss of function burden analysis study. Manhattan plot of p-values resulting from exome wide loss of function burden testing analysis for the thickness of each of the retinal layers (A) ONL, missense model, (B) IS, missense model, (C) OS, missense model, (D) ONL, loss of function model, (E) IS, loss of function model, (F) OS, loss of function model. Variants are considered significantly associated if they reach a p-value threshold of $P < 5 \times 10^{-5}$.

Table S6. List of genes associated with the thickness of the photoreceptor cell layers following exome analysis. List of genes associated with one of the three photoreceptor layers, the outer nuclear layer (ONL), inner segment (IS) and outer segment (OS) following gene burden testing. A significance threshold of $P < 5 \times 10^{-5}$ is used. For each gene the gene name and chromosome is listed. Each gene is also annotated with any prior associations to ocular and non-ocular phenotypes. The number of individuals with the homozygous loss of function allele is listed as N. Two modes were tested, a missense (MS) model and a loss of function (LoF) model.

Gene Name	N	Chr	Effect Size	P-value	Layer	Model	Ocular phenotypes	Non-ocular phenotypes
<i>TTK</i>	26	6	-0.03	1.27E-05	ONL	MS	Macular thickness	Alcoholism, Basal metabolic rate, Blood pressure, Body mass, Breast cancer, Daytime sleep phenotypes, Erythrocytes, Heel bone mineral density, Height, Lung function, Pancreatic neoplasms
<i>PGM5</i>	21	9	-0.03	4.91E-05	ONL	MS		Bipolar disorder, Blood pressure, Chronic kidney disease, Creatinine levels, Estimated glomerular filtration rate, Leg mass, Metabolite levels, Urate levels
<i>ABCA4</i>	197	1	-0.03	4.34E-05	IS	MS	AMD, Cone-rod dystrophy, Retinitis pigmentosa, Refractive error, Stargardt disease	
<i>PITX2</i>	11	4	-0.03	4.67E-05	IS	MS	Axfield Anomaly, Glaucoma, Peters anomaly, Rieger Anomaly, Ring dermoid of Cornea	Acute appendicitis, Arrhythmia, Atrial fibrillation, Hypertension, Ischemic stroke
<i>NR2E3</i>	173	15	0.03	5.42E-06	IS	MS	Abnormality of the eye, Enhanced S-Cone syndrome, Goldmann-Favre syndrome, Macular thickness, Retinitis pigmentosa, Strong/weak meridian, Vertical cup-disc ratio	Adolescent idiopathic scoliosis, Chronic obstructive pulmonary disease, Height, Lung Function, Pulse pressure, Rate of cognitive decline in mild cognitive impairment, Red blood cell count, Urate levels
<i>MYO7A</i>	350	11	0.03	3.33E-05	OS	MS	Retinal dystrophy, Retinitis pigmentosa, Usher syndrome	Allergic disease, BMI, Deafness, Educational attainment, Hand grip strength, Height, Platelet traits, Ulcerative colitis
<i>OCA2</i>	480	15	0.04	2.33E-09	OS	MS	Age-related macular degeneration, Age started wearing glasses, Corneal astigmatism, Eye colour, Macular thickness, Oculocutaneous albinism, Refractive error	ADHD, Ease of Tanning, Educational attainment, Hair colour, Malignant neoplasm of skin, Skin colour, Sunburn, Vitiligo
<i>GDPGP1</i>	50	15	0.03	2.28E-05	OS	MS	Glaucoma, IOP	Allergic disease, Eczema, Heel bone mineral density, Height, Male-pattern baldness, Multiple sclerosis, Platelet traits, Type 2 diabetes, White blood cell traits
<i>ABCD4</i>	15	14	0.03	8.52E-06	IS	LoF	Glaucoma, IOP, Macular thickness, Refractive error, Spherical power	Body mass, Depression, Educational attainment, Height, Lung function, Methylmalonic aciduria and homocystinuria, Neuroticism, Red blood cell traits
<i>CIB3</i>	10	19	-0.03	2.69E-05	IS	LoF	Myopia	Heel bone mineral density, Height, Platelet traits, Urinary metabolites, White blood cell traits

Table S7. Geneset enrichment analysis. The results of geneset enrichment analysis using DEPICT applied to the GWAS results of the meta analysed PRC layers. All genesets which were significantly enriched following correction for false discovery rate are listed below.

Original gene set ID	Original gene set description	Nominal P-value	False discovery rate <5%
GO:0000978	RNA polymerase II core promoter proximal region sequence-specific DNA binding	5.65E-07	Yes
KEGG:Circadian Rhythm Mammal	KEGG:Circadian Rhythm Mammal	8.90E-07	Yes
ENSG00000134852	CLOCK subnetwork	1.76E-06	Yes
MP:0001303	abnormal lens morphology	1.78E-06	Yes
GO:0000981	sequence-specific DNA binding RNA polymerase II transcription factor activity	3.01E-06	Yes
MP:0002840	abnormal lens fiber morphology	9.06E-06	Yes
MP:0001304	cataracts	9.17E-06	Yes
GO:0051898	negative regulation of protein kinase B signaling cascade	9.81E-06	Yes
ENSG00000151623	NR3C2 subnetwork	1.16E-05	Yes
ENSG00000162992	NEUROD1 subnetwork	1.16E-05	Yes
ENSG00000100380	ST13 subnetwork	1.28E-05	Yes
ENSG00000164442	CITED2 subnetwork	1.57E-05	Yes
MP:0001299	abnormal eye distance/ position	1.63E-05	Yes
GO:0000987	core promoter proximal region sequence-specific DNA binding	1.93E-05	Yes
GO:0001159	core promoter proximal region DNA binding	2.86E-05	Yes
MP:0001328	disorganized retinal layers	2.87E-05	Yes
GO:0071478	cellular response to radiation	3.01E-05	Yes
GO:0000982	RNA polymerase II core promoter proximal region sequence-specific DNA binding transcription factor activity	3.22E-05	Yes
GO:0043401	steroid hormone mediated signaling pathway	3.53E-05	Yes
ENSG00000031544	ENSG00000031544 subnetwork	3.58E-05	Yes
ENSG00000160202	CRYAA subnetwork	4.02E-05	Yes
GO:0034339	regulation of transcription from RNA polymerase II promoter by nuclear hormone receptor	4.38E-05	Yes
GO:0001077	RNA polymerase II core promoter proximal region sequence-specific DNA binding transcription factor activity involved in positive regulation of transcription	4.97E-05	Yes
GO:0004879	ligand-activated sequence-specific DNA binding RNA polymerase II transcription factor activity	5.58E-05	Yes
REACTOME:Nuclear Receptor Transcription Pathway	REACTOME:Nuclear Receptor Transcription Pathway	5.68E-05	Yes
GO:0003707	steroid hormone receptor activity	7.87E-05	Yes
ENSG00000126351	THRA subnetwork	1.00E-04	Yes
GO:0071482	cellular response to light stimulus	1.00E-04	Yes
ENSG00000179588	ZFPM1 subnetwork	1.06E-04	Yes
ENSG00000151090	THRB subnetwork	1.08E-04	Yes
MP:0002864	abnormal ocular fundus morphology	1.18E-04	Yes
ENSG00000108094	CUL2 subnetwork	1.28E-04	Yes
MP:0001293	anophthalmia	1.30E-04	Yes
GO:0043491	protein kinase B signaling cascade	1.34E-04	Yes
ENSG00000124151	NCOA3 subnetwork	1.35E-04	Yes
GO:0004859	phospholipase inhibitor activity	1.42E-04	Yes
MP:0002944	increased lactate dehydrogenase level	1.44E-04	Yes
ENSG00000173486	FKBP2 subnetwork	1.53E-04	Yes
GO:0009416	response to light stimulus	1.57E-04	Yes
ENSG00000116016	EPAS1 subnetwork	1.63E-04	Yes
MP:0004362	cochlear hair cell degeneration	1.63E-04	Yes
ENSG00000206289	RXRB subnetwork	1.64E-04	Yes
ENSG00000206218	ENSG00000206218 subnetwork	1.64E-04	Yes
ENSG00000204231	RXRB subnetwork	1.64E-04	Yes

Table S7. continued

GO:0043010	camera-type eye development	1.78E-04	Yes
MP:0001382	abnormal nursing	1.90E-04	Yes
MP:0000784	forebrain hypoplasia	2.14E-04	Yes
ENSG00000004059	ARF5 subnetwork	2.20E-04	Yes
GO:0000976	transcription regulatory region sequence-specific DNA binding	2.23E-04	Yes
MP:0009434	paraparesis	2.25E-04	Yes
ENSG00000139323	POC1B subnetwork	2.26E-04	Yes
GO:0009314	response to radiation	2.33E-04	Yes
GO:0030032	lamellipodium assembly	2.42E-04	Yes
MP:0008511	thin retinal inner nuclear layer	2.53E-04	Yes
GO:0055102	lipase inhibitor activity	2.83E-04	Yes
GO:0001654	eye development	2.90E-04	Yes
GO:0005212	structural constituent of eye lens	2.96E-04	Yes
GO:0007030	Golgi organization	3.11E-04	Yes
GO:0001078	RNA polymerase II core promoter proximal region sequence-specific DNA binding transcription factor activity involved in negative regulation of transcription	3.16E-04	Yes
MP:0005253	abnormal eye physiology	3.26E-04	Yes
ENSG00000132780	NASP subnetwork	3.40E-04	Yes
ENSG00000121671	CRY2 subnetwork	3.43E-04	Yes
ENSG00000173991	TCAP subnetwork	3.47E-04	Yes
MP:0005591	decreased vasodilation	3.47E-04	Yes
GO:0030275	LRR domain binding	3.53E-04	Yes
GO:0009755	hormone-mediated signaling pathway	3.54E-04	Yes
GO:0000977	RNA polymerase II regulatory region sequence-specific DNA binding	3.71E-04	Yes
ENSG00000113312	TTC1 subnetwork	3.90E-04	Yes
ENSG00000184357	HIST1H1B subnetwork	4.07E-04	Yes
MP:0002280	abnormal intercostal muscle morphology	4.14E-04	Yes

Table S8. Tissue enrichment analysis. The results of tissue enrichment analysis using DEPICT applied to the GWAS results of the meta analysed PRC layers. All Tissues which were nominally significantly enriched are listed below.

MeSH term	MeSH first level term	MeSH second level term	Nominal P value	False discovery rate <5%
A11.436	Epithelial Cells	Cells	1.17E-04	Yes
A09.371	Eye	Sense Organs	8.02E-04	Yes
A09.371.729	Retina	Sense Organs	1.64E-03	Yes
A10.615	Membranes	Tissues	4.41E-03	No
A10.615.550	Mucous Membrane	Tissues	0.01	No
A10.615.550.599	Mouth Mucosa	Tissues	0.02	No
A03.734.414	Islets of Langerhans	Digestive System	0.03	No
A14.549	Mouth	Stomatognathic System	0.04	No
A10.272	Epithelium	Tissues	0.04	No
A10.615.550.760	Respiratory Mucosa	Tissues	0.05	No
A04.531.520	Nasal Mucosa	Respiratory System	0.05	No
A09.531	Nose	Sense Organs	0.05	No

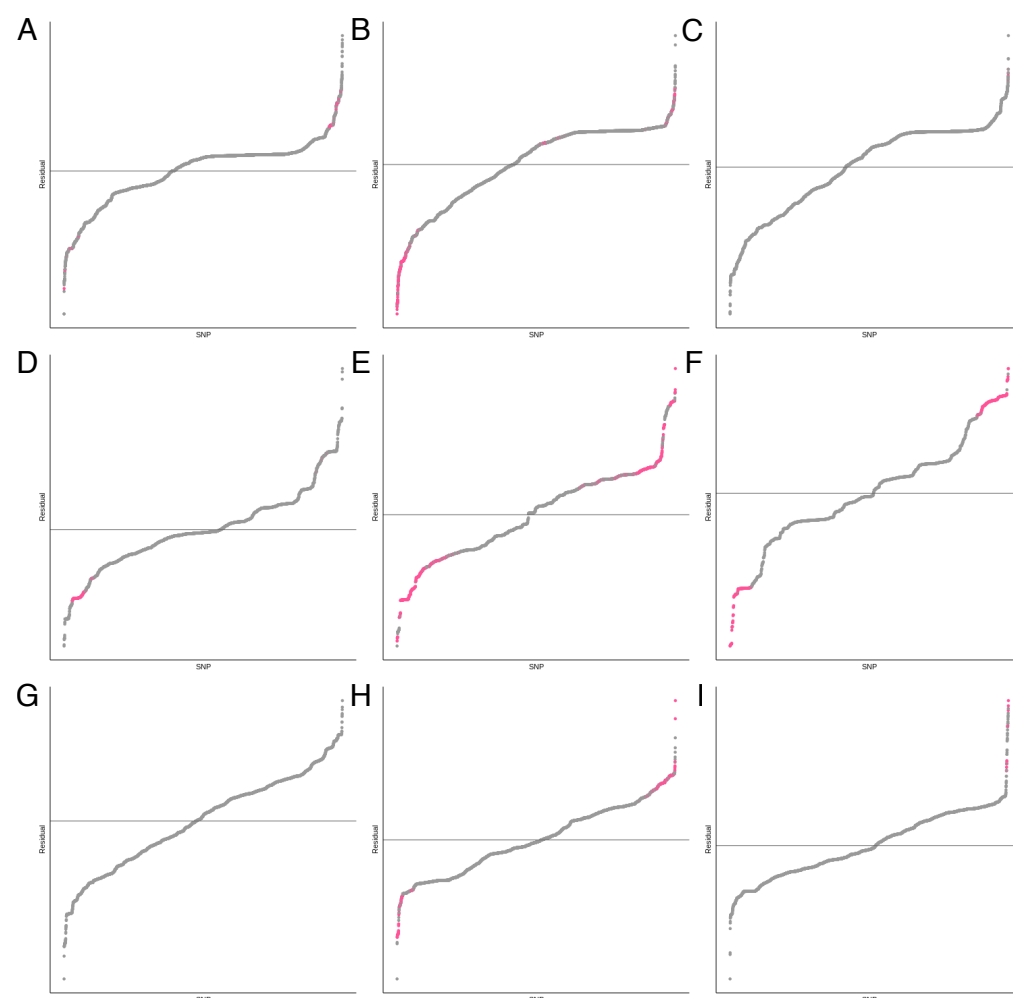


Fig S3. Comparison of the genetic effect on the thickness of concentric retinal fields. Plots depicting the residuals from models comparing the effect size of SNPs on the thickness of each retinal varinats in different concentric retinal fields. Variants with significantly different effect sizes on the two different areas tested, as determined by a z-score, are highlighted in pink. (A) ONL, fovea compared to intermediate; (B) ONL, fovea compared to peripheral; (C) ONL, intermediate compared to peripheral; (D) IS, fovea compared to intermediate; (E) IS, fovea compared to peripheral; (F) IS, intermediate compared to peripheral; (G) OS, fovea compared to intermediate; (H) OS, fovea compared to peripheral; (I) OS, intermediate compared to peripheral.

Table S9. List of SNPs differentially affecting the thickness of the ONL at the three concentric fields of the macula. List of SNPs with a significant z-score describing the differential effect on the ONL thickness at the foveal (F), intermediate (I) and peripheral (P) fields. The field (F1 or F2) and corresponding effect size from GWAS of thickness in each field are listed alongside the p-value of the comparative z-score. Each genetic variant is also annotated with associated gene and any ocular and non-ocular phenotypes previously associated with it. The different concentric comparisons are separated by bold horizontal lines.

SNP	Chr	F1	F2	F1 effect size	F2 effect size	P-value	Associated gene	Ocular phenotypes	General phenotypes
rs11708067	3	F	I	0.69	0.10	1.00E-07	<i>ADCY5</i>	Refractive error	Birth length, Birth weight, Cholesterol levels, Chronotype, Chronic kidney disease, Fasting blood glucose, Forced expiratory volume, Heel bone mineral density, Height, Type 2 diabetes
rs75757892	6	F	I	-1.12	-0.55	3.75E-06	<i>RREB1</i>	AMD, Cup-to-disc ratio, Refractive error	Birth weight, Blood glucose levels, Chronic kidney disease, Heel bone mineral density, Height, Hematocrit, Hemoglobin concentration, Impedance of body, Microcephaly, Mouth ulcers, Multiple sclerosis, Parkinsons, Red blood cell count, Self-reported math ability, Stroke, Type 2 diabetes, White blood cell count
rs45569432	14	F	I	-1.35	-2.17	3.27E-08	<i>VSX2</i>	Macular thickness, Refractive error	Cancer of endocrine glands, Chronotype, Red blood cell traits
rs1769287	1	F	P	-0.59	-0.05	6.90E-08	<i>SLC1A7</i>		Amyotrophic lateral sclerosis, Duration of fitness test, Height, Hippocampal atrophy, Lupus
rs6701735	1	F	P	0.67	-0.07	5.14E-07	<i>MIR29B2CHG</i>		Pulse rate, White blood cell count
rs11125573	2	F	P	0.54	0.08	2.27E-06	<i>CCDC88A</i>		Appendicular lean mass
rs11720108	3	F	P	0.71	-0.04	9.67E-13	<i>ADCY5</i>	Refractive error	Birth weight, Chronic kidney disease, Chronotype, Forced expiratory volume, Heel bone mineral density, Sex hormone-binding globulin levels, Statin medication, Type 2 diabetes
rs55914544	5	F	P	0.65	-0.04	2.53E-08	<i>WWC1</i>		Blood pressure, BMI, Body fat, Cerebellum cortex volume, Epithelial ovarian cancer

Table S9. continued

rs75757892	6	F	P	-1.12	-0.20	1.84E-15	<i>RREB1</i>	AMD, Cup-to-disc ratio, Refractive error	Birth weight, Blood glucose levels, Chronic kidney disease, Heel bone mineral density, Height, Hematocrit, Hemoglobin concentration, Impedance of body, Microcephaly, Mouth ulcers, Multiple sclerosis, Parkinsons, Red blood cell count, Self-reported math ability, Stroke, Type 2 diabetes, White blood cell count
6:150016812_GA_G	6	F	P	0.61	0.13	1.54E-06			
rs746173658	8	F	P	0.22	0.93	4.85E-12			
rs1337805	9	F	P	-0.52	0.06	2.07E-07	<i>PTPRD</i>	Myopia	ADHD, Anxiety, Asthma, Blood pressure, Cancer, Cholesterol, Coronary disease, Depression, Diabetes, Epilepsy, Forced expiratory volume, Heel bone mineral density, Height, Menarche
rs11594394	10	F	P	0.61	0.04	1.45E-08	<i>FRMPD2</i>	Age started wearing glasses, Myopia, Refractive error, Spherical power	
rs12225226	11	F	P	0.20	-0.45	2.33E-07	<i>LINC01488</i>		BMI, Breast cancer, Cardiomyopathy, Height, Monocyte count, White blood cell count
rs3138142	12	F	P	1.37	0.81	1.03E-07	<i>RDH5</i>	Age started wearing glasses, Cataract, Early AMD, Fundus albipunctatus, Hypermetropia, Macular thickness, Myopia, Pigmentary retinal dystrophy, Refractive error, Retinal dystrophy, Retinitis pigmentosa, Spherical power	
rs3921811	12	F	P	0.57	-0.02	7.37E-10	<i>PLEKHA5</i>		Time spent outdoors in winter
rs1493529	13	F	P	-0.48	0.07	1.05E-08	<i>ENOX1</i>		Arteries, Blood pressure, Depression, End-stage coagulation, Glucose, Mental health disorders, Prostate tumour
rs1972565	14	F	P	1.27	1.94	8.59E-09	<i>VSX2</i>	Macular thickness, Refractive error	Blood pressure, Chronotype, Coronary artery disease
rs3138142	12	I	P	1.28	0.81	1.31E-07	<i>RDH5</i>	Age started wearing glasses, Cataract, Early AMD, Fundus albipunctatus, Hypermetropia, Macular thickness, Myopia, Pigmentary retinal dystrophy, Refractive error, Retinal dystrophy, Retinitis pigmentosa, Spherical power	

Table S10. List of SNPs differentially affecting the thickness of the IS at the three concentric fields of the macula. List of SNPs with a significant z-score describing the differential effect on the IS thickness at the foveal (F), intermediate (I) and peripheral (P) fields. The field (F1 or F2) and corresponding effect size from GWAS of thickness in each field are listed alongside the p-value of the comparative z-score. Each genetic variant is also annotated with associated gene and any ocular and non-ocular phenotypes previously associated with it. The different concentric comparisons are separated by bold horizontal lines.

SNP	Chr	F1	F2	F1 effect size	F2 effect size	P value	Associated gene	Ocular phenotypes	General phenotypes
rs4721061	7	F	I	-0.23	-0.09	3.40E-11	<i>TMEM106B</i>		Coronary artery disease, Dementia, Depression, Height, Irritability, Mood swings, Neuroticism
rs55798570	10	F	I	0.13	1.61E-03	2.06E-06	<i>CDHR1</i>	Cone-rod dystrophy, Refractive error, Retinitis pigmentosa	
rs61773269	1	F	P	-0.23	-0.03	1.43E-06	<i>LRRC8D</i>		
rs7430585	3	F	P	-0.26	-0.05	1.27E-18	<i>TSC22D2</i>	Age started wearing glasses	Blood pressure, Brain morphology, Cholesterol, Platelet count, Pulse pressure, Type 2 diabetes
rs59515506	4	F	P	-0.34	-0.01	7.15E-09	<i>RUFY3</i>		Cardiovascular disease, Hippocampus, Parkinson disease
rs4131080	5	F	P	-0.12	-0.02	1.95E-06	<i>HNRNPH1</i>		Neutrophil count, White blood cell count
5:71646122_AATTT_A	5	F	P	-0.03	0.08	4.20E-07			
6:31806799_CA_C	6	F	P	-0.13	0.01	3.33E-08			
rs13237518	7	F	P	-0.23	-0.02	1.77E-26	<i>TMEM106B</i>		Coronary artery disease, Dementia, Depression, Height, Irritability, Mood swings, Neuroticism, Type 2 diabetes
rs141629142	9	F	P	0.40	0.06	9.15E-06	<i>RORB</i>	Advanced AMD, Macular thickness, Myopia, Refractive error	Alcohol consumption, Blood pressure, BMI, Cholesterol, Chronotype, Creatinine, Epilepsy, Erythrocytes, Glomerular filtration rate, Glucose, Heart failure, Height
rs1409396	10	F	P	0.13	0.02	7.63E-09	<i>PIP4K2A</i>		Frequency of walking for pleasure, Height, Platelet distribution width
rs55798570	10	F	P	0.13	-0.06	1.12E-13	<i>CDHR1</i>	Cone-rod dystrophy, Refractive error, Retinitis pigmentosa	
rs200916002	14	F	P	-0.07	-0.21	1.46E-06	<i>BBOF1</i>		
rs55634267	17	F	P	0.20	0.05	1.08E-11	<i>GNGT2</i>	Refractive error, Spherical power	Angina, Asthma, Chronic lower respiratory disease, Coronary artery disease, Eosinophil counts, Hypertension, Impedance of limbs, Metabolite errors, Prostate cancer

Table S10. continued

rs850526	17	F	P	-0.16	-0.04	7.56E-08	<i>GNGT2</i>	Spherical power, Refractive error	Appendicular lean mass, Asthma, Chronic lower respiratory disease, Metabolite levels, Primary sclerosing cholangitis, Prostate cancer
rs76076446	19	F	P	0.31	-0.09	1.76E-09	<i>RAX2</i>	AMD, Cone-rod dystrophy, Macular thickness, Retinal dystrophy	
rs2236665	21	F	P	0.16	0.01	1.53E-13	<i>RRP1B</i>	Refractive error, Spherical power	Blood pressure, Coronary artery disease, Haemoglobin traits, High blood pressure, Hypertension, Red blood cell traits
rs1041451	21	F	P	-0.14	-0.01	2.74E-10	<i>C2CD2</i>		
rs6414375	3	I	P	-0.18	-0.06	9.14E-10	<i>TSC22D2</i>	Age started wearing glasses, Glaucoma, IOP, Macular thickness, Refractive error	Blood pressure, Brain morphology, Cholesterol, Platelet count, Pulse pressure, Type 2 diabetes
rs13171669	5	I	P	-0.01	0.07	3.06E-06	<i>AFAP1L1</i>	Macular thickness	Blood pressure, BMI, Forced expiratory volume, Glomerular filtration, Hearing difficulties, Hypertension, Socioeconomic factors
rs11974335	7	I	P	-0.09	-0.01	1.15E-05	<i>TMEM106B</i>		Dementia, Depression, Height, Impedance of body, Irritability, Mood swings, Neuroticism
21:45115055_CT_C	21	I	P	0.11	0.01	8.27E-08			

Table S11. List of SNPs differentially affecting the thickness of the OS at the three concentric fields of the macula. List of SNPs with a significant z-score describing the differential effect on the OS thickness at the foveal (F), intermediate (I) and peripheral (P) fields. The field (F1 or F2) and corresponding effect size from GWAS of thickness in each field are listed alongside the Bonferroni adjusted p-value of the comparative z-score. Each genetic variant is also annotated with associated gene and any ocular and non-ocular phenotypes previously associated it. The different concentric comparisons are separated by bold horizontal lines.

SNP	Chr	F1	F2	F1 effect size	F2 effect size	P value	Associated gene	Ocular phenotypes	General phenotypes
rs1329428	1	F	P	0.64	0.24	4.79E-13	<i>CFH</i>	Advanced AMD, Chronic central serous retinopathy, Disorders of the choroid and retina	Lung function
rs200857348	2	F	P	1.45	0.60	3.96E-10	<i>MREG</i>	Macular thickness	Albuminuria, Breast neoplasms, Coronary artery disease, Heart failure, Socioeconomic factors
rs869016	2	F	P	-0.31	0.02	3.57E-09	<i>MERTK</i>	Retinitis pigmentosa	Blood pressure, Coronary artery disease, Heel bone mineral density, Multiple sclerosis
rs556679	6	F	P	0.56	0.18	8.11E-06	<i>C2</i>	AMD, Diabetic retinopathy, Other retinal disorders	Ankle spacing width, Asthma, Autoimmune disease, Body fat, Coeliac disease, Coffee consumption, Glomerular filtration rate, Membranous nephropathy, Multiple sclerosis, Psoriasis, Type 1 diabetes
rs199637836	10	F	P	-0.76	-0.24	1.38E-14			
rs3138141	12	F	P	0.76	0.32	4.48E-13	<i>RDH5</i>	Advanced AMD, Age started wearing glasses, Cataract, Fundus albipunctatus, Hypermetropia, Macular thickness, Myopia, Retinal dystrophy, Spherical power	Atrial fibrillation
rs62125245	19	F	P	0.44	0.11	7.07E-06	<i>NXNL1</i>		
rs3138142	12	I	P	0.78	0.32	3.08E-17	<i>RDH5</i>	Advanced AMD, Age started wearing glasses, Cataract, Fundus albipunctatus, Hypermetropia, Macular thickness, Myopia, Retinal dystrophy, Spherical power	Atrial fibrillation

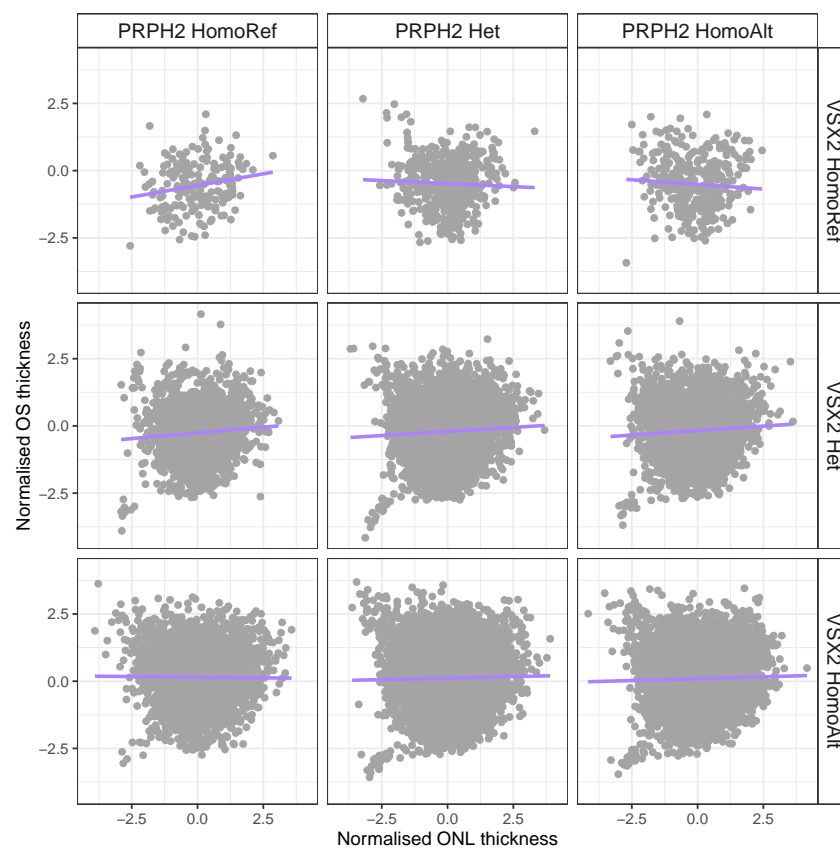


Fig S4. Interaction between genetic variants in *VSX2* and *PRPH2*.
Comparison of normalised outer segment (OS) thickness and outer nuclear layer thickness (ONL) in population subsetting by their genotype at *VSX2* (rs1972565) and *PRPH2* (rs375435).